Response to Anonymous Referee #1

This manuscript reported a positive correlation between LWP and aerosol number concentration for "dry" atmosphere condition observed during the recent CARDEX field campaign. This relationship was further explored for the low and high polluted cases separately that led to the discussion about the causal mechanisms. The analysis based on new data and the supplemental material made this manuscript valuable for the community. However, the presentation of the results was lack of coherence. A proper literature review was missing in the introduction; some figures were out of place; the key points were not presented clearly in the current manuscript, some of them were discussed back and forth with supporting material in different sections; the writing should be refined and improved. The manuscript should be accepted after some substantial revisions.

We thank the reviewer for their careful reading of our manuscript. We reproduce the reviewer comments in normal face text and respond to the each comment below in bold, with edits to passages within the text provided in *italics*.

1. In the introduction, there should be a review on the climatology and aerosol transport of this studied region. Current Figure 1 offers a big picture of the aerosol transport, but has not been discussed in details in the text. The discussion on large scale condition and aerosol origin in section 3 would have more theoretical support if the related information and previous studies were properly introduced first.

Thank you for this input. We address Comments 1 and 2 below Comment 2.

2. The introduction should also include a literature review about the past studies on aerosol to cloud properties relationship. Without literature review and comparison of this work to the previous studies, it is hard to see how this work contributes to the scientific understanding of the aerosol-cloud interaction.

We have added additional text to the introduction providing more background. New text has been added as follows:

> As nations in southeast Asia have increased bio- and fossil fuel combustion in recent decades, corresponding increases in atmospheric aerosol pollution have been seen over the region (e.g. Ramanathan et al, 2001). The high levels of anthropogenic emissions combine with the seasonal monsoon cycle (Lawrence and Lelieveld, 2010) to cause frequent episodes of heavy air pollution over the northern Indian Ocean, especially in the so-called winter monsoon season (November through March) when the low-level atmospheric flow is northerly/northeasterly, following the temperature gradient from the colder subcontinent to the warmer ocean (Figure 1).
>
> In addition to their direct effects on the climate (i.e. heating or cooling), aerosols are also known to affect clouds by three primary mechanisms: cloud brightening (e.g. Twomey, 1974, the first indirect effect); precipitation suppression (e.g. Albrecht, 1989, the second indirect effect); and radiative (the so-called semi-direct) effects, which may either enhance or diminish cloud cover based on the cloud type and relative position of the aerosol layer (e.g. Koch and Del Genio,

2010). It is important to note that in addition to the often opposing signs of each of these effects, aerosol-cloud interactions have been shown to be highly dependent on the regime (i.e. the typical meteorological conditions, cloud types, location) in which they are found (Stevens and Feingold, 2009). That is, the expression of any or multiple aerosol-cloud effects will be dependent on the conditions under which they are expressed, and thus may vary from one region to another even when considering physically similar clouds. In-situ observations of all types of clouds are thus critical to understanding the full range of indirect effects influencing the Earth's atmosphere.

3. Figures and tables from the appendix are frequently cited in the section 2 and 3, affecting the logical flow of the writing. It seems Figure A1,2,3,4,7,8,9,10, Table A1 are not cited in the appendix, but only in section 2 and 3. Appendix A may be consolidated into the method section, since it is only three paragraphs and they are closely related to the results being discussed later in the manuscript.

Thank you for this comment. We intend the appendix as a compilation of additional text as well as figures which may be of interest to those looking for more depth on our work, without being a primary result of the paper. The Appendix figures and the Appendix text are thus intended to be largely exclusive of one another. However, we have rewritten references in Sections 2 and 3 to highlight the figures of the main text while using the appendix as a supplement where appropriate, and have done some minor reorganizing within the figures (e.g. we have consolidated the original Fig. 7 and A5 into one, and moved Figure 7 after Figure 10 while removing Figure 8 as addressed in a later comment). We have rewritten the text referencing the appendix figures to make them more concise and stand-alone as a supplement. Regarding Appendix A, we have added some additional methods text in the revision and believe it remains long enough and specific enough to merit its own appendix. The revised intro text laying out the paper structure is copied below:

> Here we present new observations of the dry season climatology of this trade cumulus regime, including cloud, aerosol, and meteorological properties, as observed during CARDEX. In Sect. 2, we *describe characteristics of the full CARDEX dataset* and two distinct *classes of* atmospheric properties ("wet" and "dry" regimes) *and examine* the differing *conditions which are responsible for each*. *Section 3 then focuses on cases within the latter regime to describe the systematic distinctions observed between low and high pollution cases, as well as observed aerosol–cloud correlations. These pollution case studies allow insight into the mechanisms governing the observed differences in cloud properties*. We then offer *a brief discussion of* some potential causal factors of the observed correlations, including the role of aerosol in modifying atmospheric humidity and the potential implications for the understanding of aerosol effects on clouds.

4. Since the moderately polluted cases contribute to nearly half of the total cases, the results from these cases should be at least discussed in the manuscript, and compared to the low- and high-polluted cases.

This was discussed in the original text (Page 29355, Lines 22-25; Table 4). As mentioned in the text, we wish to focus on the contrast between the two case studies; however, we have added brief additional text describing the characteristics of Case M as follows:

> The ``moderately polluted'' cases (1000<CPC<1500,cm^{-3}) are excluded from the figures in order to bring focus to the high/low pollution contrast; however, Table 4 shows that these observations consistently fall between Case L and Case H *(e.g. LWP, z_PBL, LEF),* and in many cases they are in fact closer to Case H values *(e.g. LCL, z_cb, humidity)*. *This holds true for the UAV vertical profiles (T, RH, aerosol) as well.*

5. Have the authors explored the reasons why the "wet" cases do not show a correlation between LWP and CPC? This seems to be an important piece of the puzzle, and could potentially help to explain the correlation shown in the "dry" cases.

Thank you for this comment. The main point of making this distinction is that LWP exhibits much greater variability during the "wet" periods, (evident in Figure 6 and Table 3); therefore a longer record of LWP data would be required to detect a statistically significant correlation for those cases. Thus while the focus of this paper is on the variability under the so-called dry cases, we have added additional text regarding our hypothesis as to the ''wet''/LWP correlations.

> This difference in origin corresponds to greater variability in the clouds formed during "wet" conditions. When considering only the "dry" cases *with a narrower range of variability in LWP*, we *are able to detect a statistically-significant correlation between aerosol and cloud variability*. *We hypothesize that the greater variability of LWP under high-humidity conditions is a result of unconstrained vertical development of the clouds which form under more humid conditions; greater humidity tends to increase cloud thickness, so greater upper-level humidity may feed cloud development that is decoupled from conditions within the boundary layer.*

6. Figure 8 seems redundant after Figure 7.

The original Figure 8 has been removed and the discussion has been consolidated around original Figure 7.

> Figure *9 [original Figure 7]* shows the observed Case L and Case H 5 flight profiles from the aerosol-radiation UAV. Note that Case H is uniformly more polluted (as measured by both the CPC and aethalometer) through the lower atmosphere up to about 2km, at which point average pollution decreases for both cases. This is true for all cases except for one Case L flight which sampled an elevated aerosol plume. Case H exhibits warmer temperatures throughout the atmospheric column, with the maximum mean difference between the two cases occurring around the temperature inversion/cloud layer altitude (due to systematic differences in inversion height for Case L vs. H*).* […] The more polluted cases rather uniformly have higher boundary-layer relative humidity, and substantially higher free troposphere relative humidity. *The brief exception to this is around 800m, where the humidity of Case L is greater than that of Case H; this* corresponds to differences in the average altitude of the sub-cloud mixed layer

between the two cases, which is higher in altitude for Case L. Case H again has higher RH above the inversion, which may partly facilitate the correspondingly larger average cloud water content in this case, *similar to the hypothesized mechanism behind the variability in cloud liquid water for the "wet" versus "dry" cases as discussed in Section 2, though to a lesser degree.*

7. The air mass back trajectories are mentioned in section 2.2, and the air mass origin is again discussed in section 3.2.2. The authors should consider rearrange and consolidate the material.

Thank you for the comment. As also addressed under Comment #3, the structure of the paper was intended to first discuss the dataset as a whole in Section 2 (i.e. the wet/dry distinction), before focusing solely on the ''dry'' data in Section 3. Additionally, the discussion in Section 3 has been substantially rearranged for clarity. Specifically, Section 3.1 has been rearranged in itself; text from Section 3.3 has been moved up to 3.1; the remaining Section 3.3 has been rearranged. The difference in the context between the air mass trajectories in Section 2.2 and Section 3.2.2 has been clarified.

1. Page 29349, line 7, change to "INDOEX is the result of…"

This has been reworded to improve clarity. The sentence now reads:

INDOEX, a collaborative experiment between multiple international organizations and led by Scripps Institution of Oceanography, made simultaneous multi-platform measurements in the Indian Ocean with the goal of observationally constraining direct and indirect effects of aerosols in the region, in particular the atmospheric heating and surface cooling caused by the presence of black carbon (BC) aerosols within the atmospheric column.

2. Page 29349, line 16, delete "would"

This has been changed for clarity.

INDOEX *thus* set the stage for later work in the region investigating the effects of absorbing aerosols within the atmospheric column.

3. Page 29349, line 25, "CARDEX follows…" should be moved to the next paragraph

This sentence has been reworded as follows, however it should remain as the concluding sentence of the previous paragraph as it functions as a transitional concluding sentence.

CARDEX follows from these previous studies using UAVs and ground measurements, and for the first time incorporates *measurements of turbulent kinetic energy and latent heat fluxes* for a greater focus on *how thermodynamic factors and atmospheric dynamics* may *influence aerosol effects on clouds*.

4. Page 29350, line 16, delete "a time"

We believe "a time" is necessary for grammatical clarity of this phrase (i.e. we are saying "the dry season is a time when…" rather than "CARDEX was designed when…").

5. Page 29350, line 17 to 20, “The atmospheric conditions…” please rephrase this sentence

The sentence has been reworded as follows

> *As the atmosphere is heavily influenced by anthropogenic pollution during this dry season, the data presented here are valuable to a broader understanding of potential aerosol effects on atmospheric conditions.*

6. Page 29350, line 28, “discussion” seems to be a more suitable word instead of “speculation”

This has been changed.

> We then offer *a* brief *discussion of* some potential causal factors of the observed correlations, including the role of aerosol in modifying atmospheric humidity and the potential implications for the understanding of aerosol effects on clouds.

7.Page 29353, line 14 to 19 need to be rephrased.

We have restructured this paragraph and reworded the sentences for clarity as follows:

> *Thus the most significant distinction in the atmospheric structure of the two populations is in the conditions above the boundary layer, especially the lack of temperature inversion and greater atmospheric humidity at higher elevations for the ``wet'' cases. This analysis is additionally supported by the ECMWF reanalysis over MCOH (Fig. A3a and b).*
>
> *Note that the atmospheric moisture described here is given as relative humidity (RH), as this is the metric directly measured by the aircraft. Although an increase in temperature would produce a decrease in RH for a fixed specific humidity (q), in our cases the measured RH is seen to be consistent with q calculated incorporating changes in temperature (e.g. Fig.A5).*

8. Page 29355, line16, change to “all available low/high pollution dry days”

This has been reworded for clarity.

> In this analysis, we use all low/high pollution dry days *with available reanalysis and satellite data (Table 1)*; observations from the UAVs are necessarily limited to the subset of these days when a UAV was flown (Table 2).

9. Page 29360, line 2, this sentence “The bottom: : :” is not necessary

This sentence has been removed.

10. Page 29361 line 26, delete one of the “in contrast to the”

Thank you for catching this typo! It has been removed.

Response to Anonymous Referee #2

Pistone et al. present data and analysis of aerosol, cloud and meteorological data in a trade wind regime over the Indian Ocean. Its subject and content is surely of interest to ACP. Here are some comments for the authors and the editor to consider.

We thank this reviewer for their careful reading of our manuscript. Responses to comments (reproduced as normal face text) are given below in bold, with edits to passages within the text provided in *italics*.

Major comments:

1. The abstract needs to be rewritten. I think it can be more specific and to the point. In particular, they could highlight the uncertainties involved in the interpretation of the results they have.

Thank you for the comment, we have revised the abstract as follows:

> There are many contributing factors which determine the micro- and macrophysical properties of clouds, including atmospheric *vertical* structure, dominant meteorological conditions, and aerosol concentration, all of which may be coupled to one another. In the quest to determine aerosol effects on clouds, these potential relationships must be understood. Here we describe several observed correlations between aerosol conditions and cloud and atmospheric properties in the Indian Ocean winter monsoon season.
>
> In the CARDEX (Cloud, Aerosol, Radiative forcing, Dynamics EXperiment) field campaign conducted in February and March 2012 in the northern Indian Ocean, continuous measurements *were made* of atmospheric precipitable water vapor and the liquid water path (LWP) of trade cumulus clouds, concurrent with measurements of water vapor flux, cloud and aerosol vertical profiles, meteorological data, and surface and total-column aerosol. *We present observations indicating* a positive correlation between aerosol and cloud LWP which becomes clear only after the data are filtered to control for the natural meteorological variability in the region.
>
> We then use the aircraft and ground observatory measurements to explore *possible* mechanisms behind the observed aerosol–LWP correlation. *High pollution is found to correlate with higher temperatures and higher humidity measured throughout the boundary layer. The increase in cloud liquid water is found to coincide with a lowering of the cloud base resulting from the increased boundary-layer humidity. Large-scale analysis corroborates these co-variations: high pollution cases are shown to originate as a highly-polluted boundary layer air mass approaching the observatory from a northwesterly direction. This polluted mass exhibits higher temperatures–potentially attributable to aerosol absorption of solar radiation over the subcontinent–and higher humidity than the cleaner cases. While high aerosol conditions are observed to disperse with air mass evolution, along with a weakening of the high-temperature*

anomaly, the high humidity condition was observed to instead strengthen in magnitude coincident with the polluted air mass. Potential causal mechanisms of the observed correlations are then explored, though future research will be needed for a more complete and quantitative understanding of the aerosol–humidity relationship.

2. In the introduction, the material is almost exclusively about previous studies done in the Indian Ocean region, which is perfectly fine since that is the place where this experiment took place. However, since the authors also emphasize a view on the general aerosol-cloud interaction problem within the trade cumulus regime, references and discussions about other papers may be needed to put current study in a proper context.

Following this comment and the comment of Reviewer #1, we have added additional background text to the introduction:

As nations in southeast Asia have increased bio- and fossil fuel combustion in recent decades, corresponding increases in atmospheric aerosol pollution have been seen over the region (e.g. Ramanathan et al, 2001). The high levels of anthropogenic emissions combine with the seasonal monsoon cycle (Lawrence and Lelieveld, 2010) to cause frequent episodes of heavy air pollution over the northern Indian Ocean, especially in the so-called winter monsoon season (November through March) when the low-level atmospheric flow is northerly/northeasterly, following the temperature gradient from the colder subcontinent to the warmer ocean (Figure 1).

In addition to their direct effects on the climate (i.e. heating or cooling), aerosols are also known to affect clouds by three primary mechanisms: cloud brightening (e.g. Twomey, 1974, the first indirect effect); precipitation suppression (e.g. Albrecht, 1989, the second indirect effect); and radiative (the so-called semi-direct) effects, which may either enhance or diminish cloud cover based on the cloud type and relative position of the aerosol layer (e.g. Koch and Del Genio, 2010). It is important to note that in addition to the often opposing signs of each of these effects, aerosol-cloud interactions have been shown to be highly dependent on the regime (i.e. the typical meteorological conditions, cloud types, location) in which they are found (Stevens and Feingold, 2009). That is, the expression of any or multiple aerosol-cloud effects will be dependent on the conditions under which they are expressed, and thus may vary from one region to another even when considering physically similar clouds. In-situ observations of all types of clouds are thus critical to understanding the full range of indirect effects influencing the Earth's atmosphere.

3. Frankly, the organization of the manuscript is a bit loose. I would encourage the authors to better organize the material if they can.

Following this and the comments of Reviewer #1, we have re-organized and clarified the paper structure. In addition to revising the references to the Appendix throughout the paper as detailed in the Response to Reviewer #1, we have consolidated some of the discussion of Section 3.3 with that in Section 3.1, and have improved transition sentences between each section to better clarify the intended structure of the paper and to highlight the linkages between successive sections.

Minor comments:

1. Abstract Line 3: what is 'atmosphere structure' ?

This was meant to refer to atmospheric vertical structure, i.e. how atmospheric properties vary with altitude. The text has been revised to clarify this.

> …including atmospheric *vertical* structure, dominant meteorological conditions, and aerosol concentration…

2. Sentence beginning at Line 25 of Abstract: rewrite this sentence. I had a hard time understanding it.

This part of the abstract has been revised as follows:

> *While high aerosol conditions are observed to disperse with air mass evolution, along with a weakening of the high-temperature anomaly,* the high humidity condition was observed to *strengthen in magnitude as the polluted air mass moves over the ocean toward the site of the CARDEX observations*.

3. 2nd paragraph in Introduction: flux measurement is more relevant to thermodynamics instead of dynamics.

This sentence has been clarified:

> CARDEX follows from these previous studies using UAVs and ground measurements, and for the first time incorporates *measurements of turbulent kinetic energy and latent heat fluxes* for a greater focus on *how thermodynamic factors and atmospheric dynamics* may *influence aerosol effects on clouds*.

4. P29355 Line 8: using linear correlation statistics on log of data is weird. The usual assumption involved in the correlation could be violated in this case and the statistical significance test is meaningless. How about a regular linear correlation? What are the statistics for that?

Thank you for this comment. The observed LWP follows a roughly lognormal distribution, rather than normal; thus taking the log(LWP) values should result in a more normal distribution. The y-axis is illustrated as a logarithmic scale for clarity to the reader. We have also explored other metrics of statistical significance with and without the transform, and added this discussion in the text as follows:

> *However, when the data are filtered to take into account meteorology, there is a positive correlation between LWP and aerosol which is significantly greater than zero (Spearman ρ = 0.48; Pearson R = 0.42, both at the 95% confidence level) for the "dry" (PWV < 40 kg/m^2) cases only (Fig. 6b). Note that for the Pearson correlation analysis we have taken the logarithmic transform of the LWP as these data exhibit a lognormal rather than normal distribution; the non-parametric Spearman coefficient is insensitive to the logarithmic transform.*

5. Last paragraph on P29358: there is no reason to expect this island is representative of the large scale.

We agree, and believe our findings in fact indicate that the island is not representative; however, we find conditions at MCOH to be influenced by variations in large-scale conditions, and we consider it important to compare the observations made here to the larger context in which they were made. This sentence (p. 29358, lines 22-24 in the original text) reads "the pollution level classifications as determined by the conditions over MCOH are not necessarily representative of the region as a whole."

6. Sentence beginning at line 13 of P 29359: rewrite it. I could not understand it.

This sentence has been rewritten for clarity as follows:

> *Although this divergence may act to dilute the polluted air mass, the MODIS AOD shown here suggests that dilution is not the dominant factor distinguishing the two cases. Rather, polluted air is prevented from arriving at MCOH during the low pollution cases due to differences in advection patterns.*

7. Line 26 of the same page: This indicates more of an advection process.

Thank you for this comment. With Section 3.2 as a whole, it was our intention to establish that this coincidently high-aerosol, high-temperature air mass was in fact advected from the Indian subcontinent (and subsequently dispersed through the region), with aerosol heating beginning over the subcontinent (e.g. original draft, p. 29359, lines 21-24). This has been clarified in this section of the text.

> *Rather, polluted air is prevented from arriving at MCOH during the low pollution cases due to differences in advection patterns.* […] Similar to the patterns in the MODIS AOD, the high temperatures in Case H are seen to be concentrated in a region which approaches MCOH from the north, and then slightly dissipates over the four days in question *as the polluted air mass is advected southward*. The remarkable spatial coincidence of temperature with the maximum AOD *over all three days* is strongly suggestive of heating of the air mass due to absorbing aerosol, likely occurring since before the air mass leaves the subcontinent.

8. Line 7 of P 29360: how this correlation is done exactly? It needs to be clearly described. It is very important.

Thank you for the comment. We have clarified these correlations, their analysis, and discussion of their significance.

> For both pollution cases, Fig. 12 shows a region of statistically-significant correlation (95% level, indicated by hatching) between AOD and T. *These correlation coefficients (and those in Fig. 13 [original Figure 14]) were determined by calculating the Pearson correlation R between AOD and T for all days in question (i.e. all H days, or all L days), for each individual 1x1-degree*

latitude/longitude point. Finally, points were only classified as ``significant'' if there were no more than 10% of MODIS retrievals missing. While both Case L and Case H are shown for comparison, it should be noted that due to availability of fewer Case L days being observed (Table 1), the correlations for Case H (left panel) are considered more robust. Analysis for all days indicates a similar pattern to Case H, although weaker in magnitude.

The region of high positive and significant correlation *for Case H* is present over *a broad extent of* the Arabian Sea (the low-level source region to MCOH). The correlation weakens in both magnitude and area of significance between Day H-2 and Day H, which further suggests a dispersion of the polluted air mass *with time, consistent* with the above interpretation of Fig. 11. Case L *shows* a *smaller region of positive correlation concentrated to the north in* the Arabian Sea, *suggesting that while high pollution and temperature are again coincident, the polluted air mass simply is not advected in the direction of MCOH in these cases*.

9. Section 3.2.2: there are many places where correlation is negative. Given the authors' hypothesis there should be no negative correlations anywhere.

With regard to the interpretation of Figure 12, this is addressed in (original manuscript) p. 29360, lines 22-27. Our hypotheses concern vertically-coincident aerosol and meteorological conditions, whereas the region of negative correlation to the east of the subcontinent was likely a result of elevated plumes producing surface cooling. Other regions of negative correlation were not found to be statistically significant, and are likely the result of noise. We have expanded and clarified this discussion.

The smaller region of significant negative correlation to the east of the subcontinent *(particularly evident in Case H)* may be explained by low atmosphere/surface dimming due to *high AOD here indicating* an elevated aerosol plume *rather than the high boundary-layer aerosol responsible for the positive correlation to the northwest*; at higher altitudes, for example at 875 hPa (z~1250m), the AOD and temperature T_{875} show a strong positive correlation in this region. Elevated aerosol plumes are generally seen to approach MCOH from this direction, following the upper-level wind field, consistent with the findings of Höpner et al (2016).

10. Line 7 of P 29363: there are so many meteorological factors to be examined. For example, advection is not considered and it is quite relevant.

We apologize that this was not clear. The intent of this section was not to completely rule out the role of meteorology (including advection), but rather to indicate that with the present analysis, we were not able to determine that this was a dominant factor. For example, the passage immediately preceding this comment presents data which strongly suggests direct advection of high-humidity air is not primarily responsible for the observed patterns. This section has been reworded make this point more clear.

This leaves large-scale factors *(e.g. advection of warm, humid, and polluted air masses)*, local top-of-boundary-layer fluxes, or possible aerosol-induced effects as potential contributing factors to the observed higher relative humidity.

To assess the possible influence of large-scale meteorological conditions on humidity, we *examine* HYSPLIT back trajectories *for any systematic differences in the origin or evolution of the air masses for each case. These* show the upper-level flow *approaching from the northeast* over the subcontinent, consistent with the results shown in Section 2 *(Fig. 5b).* The near-surface flow originates generally from the north/northwest *for both cases; although* low pollution conditions exhibit less extended back trajectories (i.e. lower wind speed above the boundary layer), they come from generally the same direction.

Thus we found no clear meteorological distinction *(in terms of humidity level or origin)* between the two cases which might explain the difference between their boundary-layer conditions. While meteorological conditions may be a potential causal factor of the observed correlation between aerosol and cloud properties (e.g. Mauger and Norris, 2007, 2010), the present observations are not sufficient to definitively establish or discard this hypothesis. Further study of the large-scale context is necessary to more fully explore the potential meteorological influences on the low/high pollution distinction and on the aerosol–humidity relationship.

11. Line 7 of P 29364: increasing T will strongly decrease RH.

We apologize that this was not clear. While we agree that increased T would decrease local RH, this line refers to the possibility that temperature-induced changes in dynamics could potentially change large-scale transport patterns leading to advection of high-humidity air from elsewhere. This section is intended to offer potential explanations for the observed correlations—observations which show increased T to be coincident with increased RH. We have revised this section to make this point more clear.

Another possible mechanism to explain the high humidity relates to the temperature/aerosol relationship. While the *observed* development of the AOD-T relationship *(Figs. 11 and 12)* is consistent with that of aerosol heating of the air mass (Ramanathan et al, 2007), there are two possible interpretations of *how this may relate to the development of high humidity conditions.* First, the humidification of the boundary layer may *be a result of* the meteorological history of the air mass coincident with aerosol conditions (e.g. Mauger and Norris, 2007); second, aerosol conditions may be directly or indirectly increasing the boundary layer humidity. *As shown above, the first interpretation is not supported by the present study, though a more complete analysis is necessary. Regarding the second possibility, aerosol heating may suppress turbulent mixing and stabilize the boundary layer, lowering BL height and inducing higher relative humidity as the polluted plume ages. Alternately, the presence of aerosol heating within the more polluted air mass may be altering the mesoscale circulation to bring more moist air to the region.* Again, further study is needed to establish the plausibility of these potential causal mechanisms, *and to determine* whether meteorological or aerosol mechanisms may be primarily responsible for the

observed correlations. *Regardless of their mechanism, these correlations must* be considered in such studies of aerosol–cloud interactions, as secondary changes in atmospheric properties – either directly by aerosol effects or coincident with high-pollution conditions – may alter the effective magnitude of indirect effects.

12. Conclusion: it's overall too general and should be more specific.

Thank you for this comment. We have revised the conclusion as follows:

Here we have presented new results on the characterization of trade cumulus clouds and the dry season cloud climatology in the northern Indian Ocean *using combined ground station observations, vertical atmospheric profiles from UAVs, and large-scale satellite data and meteorological reanalysis*. We describe the general characteristics of the atmosphere in the region and illustrate the existence of two separate climatologies based on the water vapor conditions in the atmospheric column, which result in different populations of clouds forming: *"dry" conditions result in clouds which tend to be constrained by a well-defined boundary layer topped by an inversion, whereas the clouds forming under "wet" conditions exhibit more unconstrained and varied development fed by the availability of more humid upper-layer air.* When the data are *analyzed* according to this climatological separation to *filter out* the large natural variability of high-vapor conditions, we observe a distinct positive correlation between aerosol concentration and cloud liquid water. Highly polluted conditions *(with a high concentration of absorbing aerosol) are found* to be systematically warmer and more humid, *as seen by the ground, aircraft, and large-scale analyses*. From the in-situ aircraft and remote-sensed ground observations, we observe a lower boundary layer height under polluted cases, resulting in a lower cloud base which is responsible for the greater cloud liquid water. *The observed increase in RH was the only potential factor which could account for the magnitude of the observed greater polluted cloud LWP which results from this lower cloud base*. The large-scale analysis indicates that highly polluted air masses exiting the subcontinent are also warmer *initially*, while high-humidity conditions develop along with the air mass as it ages.

While *the strong correlation between aerosol and temperature is likely* attributable to aerosol heating of the air mass (e.g. Ramanathan et al, 2007), with the given observations we are unable to definitively determine a causal mechanism responsible for the observed *correlation between aerosol and humidity. Possible mechanisms which may be producing these correlations include meteorological or aerosol-driven factors, though we were not able to attribute the observed differences to differences in large-scale advection patterns. There remains the possibility that aerosol effects may be driving the observed lagged humidification of the boundary layer, either by influencing the mesoscale circulation or stabilizing the boundary layer locally; this is an intriguing avenue for further study.*

Understanding the consequences of aerosol—cloud interactions in this region requires an understanding of how variations in atmospheric conditions such as temperature and humidity may impact cloud dynamics and water content. Additionally, future research aiming at

understanding aerosol--cloud interactions as a whole, and effects of aerosols influencing atmospheric dynamics specifically, should incorporate both local observations of the instantaneous vertical structure and motion of the atmosphere, as well as large-scale observations to understand the air mass history and the potential influence of meteorology on these effects.

Manuscript prepared for Atmos. Chem. Phys. Discuss.
with version 2015/04/24 7.83 Copernicus papers of the LaTeX class copernicus.cls.
Date: 26 February 2016

Observed correlations between aerosol and cloud properties in an Indian Ocean trade cumulus regime

K. Pistone[1,a], P. S. Praveen[1,b], R. M. Thomas[1,c], V. Ramanathan[1], E. Wilcox[2], and F. A.-M. Bender[3]

[1]Scripps Institution of Oceanography, University of California at San Diego, La Jolla, CA, USA
[2]Desert Research Institute, Reno, NV, USA
[3]Department of Meteorology and Bolin Center for Climate Research, Stockholm University, Stockholm, Sweden
[a]now at: NASA Ames Research Center, Moffett Field, CA, USA; Universities Space Research Association, Columbia, MD, USA
[b]now at: International Centre for Integrated Mountain Development, Kathmandu, Nepal
[c]now at: School of Geography, Earth and Environmental Sciences, University of Birmingham, Birmingham, UK

Correspondence to: K. Pistone (kristina.pistone@fulbrightmail.org)

Abstract

There are many contributing factors which determine the micro- and macrophysical properties of clouds, including atmospheric vertical structure, dominant meteorological conditions, and aerosol concentration, all of which may be coupled to one another. In the quest to determine aerosol effects on clouds, these potential relationships must be understood~~, as changes in atmospheric conditions due to aerosol may change the expected magnitude of indirect effects by altering cloud properties in unexpected ways~~. Here we describe several observed correlations between aerosol conditions and cloud and atmospheric properties in the Indian Ocean winter monsoon season.

In the CARDEX (Cloud, Aerosol, Radiative forcing, Dynamics EXperiment) field campaign conducted in February and March 2012 in the northern Indian Ocean, continuous measurements were made of atmospheric precipitable water vapor and the liquid water path (LWP) of trade cumulus clouds~~were made~~, concurrent with measurements of water vapor flux, cloud and aerosol vertical profiles, meteorological data, and surface and total-column aerosol. ~~Here we present evidence of~~ We present observations indicating a positive correlation between aerosol and cloud LWP which becomes clear only after the data are filtered to control for the natural meteorological variability in the region.

We then use the aircraft and ground observatory measurements to explore ~~the~~ possible mechanisms behind the observed aerosol–LWP correlation. ~~We determine that increased boundary-layer humidity lowering the cloud base is responsible for the observed~~ High pollution is found to correlate with higher temperatures and higher humidity measured throughout the boundary layer. The increase in cloud liquid water is found to coincide with a lowering of the cloud base resulting from the increased boundary-layer humidity. Large-scale analysis ~~indicates that~~ corroborates these co-variations: high pollution cases ~~originate with a~~ are shown to originate as a highly-polluted boundary layer air mass approaching the observatory from a ~~–~~northwesterly direction. This polluted mass exhibits higher ~~temperatures and humidity than the clean case, the former of which may be attributable to heating due to~~ temperatures–potentially attributable to aerosol absorption

of solar radiation over the ~~subcontinent~~subcontinent–and higher humidity than the cleaner cases. While high ~~temperature conditions dispersed along with the high-aerosol~~ aerosol conditions are observed to disperse with air mass evolution, along with a weakening of the high-temperature anomaly, the high humidity condition was observed to ~~instead develop along with~~ strengthen in magnitude as the polluted air mass ~~. We then explore potential~~ moves over the ocean toward the site of the CARDEX observations. Potential causal mechanisms of the observed correlations are then explored, though future research will be needed ~~to more fully describe~~ for a more complete and quantitative understanding of the aerosol–humidity relationship.

1 Introduction

~~The~~ As nations in southeast Asia have increased bio- and fossil fuel combustion in recent decades, corresponding increases in atmospheric aerosol pollution have been seen over the region (e.g. Ramanathan et al, 2001) . The high levels of anthropogenic emissions combine with the seasonal monsoon cycle (Lawrence and Lelieveld, 2010) to cause frequent episodes of heavy air pollution over the northern Indian Ocean~~is a region of great interest in aerosol studies, due to frequent episodes of polluted air arriving from the Indian subcontinent.~~ , especially in the so-called winter monsoon season (November through March) when the low-level atmospheric flow is northerly/northeasterly, following the temperature gradient from the colder subcontinent to the warmer ocean (Figure 1).

In addition to their direct effects on the climate (i.e. heating or cooling), aerosols are also known to affect clouds by three primary mechanisms: cloud brightening (e.g. Twomey, 1974, the first indirect effect) ; precipitation suppression (e.g. Albrecht, 1989, the second indirect effect) ; and radiative (the so-called semi-direct) effects, which may either enhance or diminish cloud cover based on the cloud type and relative position of the aerosol layer (e.g. Koch and Del Genio, 2010) . It is important to note that in addition to the often opposing signs of each of these effects, aerosol-cloud interactions have been shown to be highly dependent on the regime (i.e.

the typical meteorological conditions, cloud types, location) in which they are found (Stevens and Feingold, 2009) . That is, the expression of any or multiple aerosol-cloud effects will be dependent on the conditions under which they are expressed, and thus may vary from one region to another even when considering physically similar clouds. In-situ observations of all types of clouds are thus critical to understanding the full range of indirect effects influencing the Earth's atmosphere.

The current study builds upon a long history of aerosol studies in the ~~region~~northern Indian Ocean, starting with the Indian Ocean Experiment (INDOEX), a collaborative multi-platform experiment in 1998–1999 ~~(Ramanathan et al, 2001) . INDOEX, the result of collaboration between multiple international organizations~~ involving scientists from several international organizations and led by Scripps Institution of Oceanography ~~, made (Ramanathan et al, 2001) . In INDOEX,~~ simultaneous multi-platform measurements were made in the Indian Ocean with the goal of observationally constraining direct and indirect effects of aerosols in the region, in particular the atmospheric heating and surface cooling caused by the presence of black carbon (BC) aerosols within the atmospheric column. The intensive field operations allowed scientists to, for the first time, quantify the direct radiative effects of absorbing aerosols originating in southeast Asia, and contrast the highly-polluted conditions north of the ITCZ with pristine Southern Hemisphere conditions (e.g. Heymsfield and McFarquhar, 2001). INDOEX ~~would~~ thus set the stage for later work in the region investigating the effects of absorbing aerosols within the atmospheric column.

The 2006 Maldives Autonomous unmanned aerial vehicle Campaign (MAC) investigated the role of absorbing aerosols in the Indian Ocean, and their effects on clouds, using lightweight unmanned aerial vehicles (UAVs) with miniaturized radiation, aerosol, and cloud instrumentation as payload (Ramanathan et al, 2007; Ramana et al, 2007; Corrigan et al, 2008; Roberts et al, 2008). The UAVs were flown stacked one on top of the other and, with their upward- and downward-looking instrumentation operating simultaneously, directly measured the amount of radiation absorbed within an aerosol layer (Ramanathan et al, 2007). CARDEX follows from these previous studies using UAVs and ground measurements, and for the first time incorporates ~~flux measurements~~ measurements of turbulent

kinetic energy and latent heat fluxes for a greater focus on ~~dynamics and how aerosol may be influencing~~ how thermodynamic factors and atmospheric dynamics may influence aerosol effects on clouds.

Between 16 February and 30 March 2012, the Cloud, Aerosol, Radiative forcing, and Dynamics EXperiment (CARDEX) was conducted on Hanimaadhoo Island, Maldives (Fig. 1), led by scientists from Scripps Institution of Oceanography in San Diego, California and including collaborators from the Desert Research Institute in Reno, Nevada; Stockholm University in Stockholm, Sweden; Max Planck Institute for Chemistry in Mainz, Germany; and Argonne National Lab in Argonne, Illinois. The Maldives Climate Observatory at Hanimaadhoo (MCOH) has been making continuous measurements of aerosol, radiation, and meteorological parameters on Hanimaadhoo Island since October 2004 (Ramana and Ramanathan, 2006). During the CARDEX campaign, measurements from small aircraft were supplemented with the continuous ground measurements at MCOH, including additional instruments exclusive to the CARDEX period: a mini-micropulse lidar (MPL) ~~,~~ to measure cloud base height, boundary layer height, and the altitude of elevated aerosol plumes; ~~and~~ a fast response water vapor sensor and gust probe (identical to those on the aircraft) to measure turbulent kinetic energy and latent energy fluxes; and a microwave radiometer (MWR) ~~,~~ to measure total-column precipitable water vapor and cloud liquid water path. CARDEX was designed to observe the atmosphere at the end of the so-called dry season (winter monsoon), a time when atmospheric flow over the Maldives is predominantly from the highly-polluted Indian subcontinent with little wet removal due to rainfall. ~~The atmospheric conditions in this season are~~ As the atmosphere is heavily influenced by anthropogenic pollution ~~, and thus the site, and this study,~~ during this dry season, the data presented here are valuable to a ~~broader~~ understanding of ~~aerosol effects~~potential aerosol effects on atmospheric conditions.

Here we present new observations of the dry season climatology of this trade cumulus regime, including cloud, aerosol, and meteorological properties, as observed during CARDEX. In Sect. 2, we describe ~~two distinct categories~~ characteristics of the full CARDEX dataset and two distinct classes of atmospheric properties ~~, here termed~~ (“wet” and “dry”

regimes~~, and explain~~) and examine the differing conditions ~~resulting in each. In Sect. 3 , we describe the aerosol–cloud correlations which were observed in CARDEX and use the systematic distinctions~~ which are responsible for each. Section 3 then focuses on cases within the latter regime to describe the systematic distinctions observed between low and high pollution cases~~to gain~~ , as well as observed aerosol–cloud correlations. These pollution case studies allow insight into the mechanisms governing the observed differences in cloud properties. We then offer ~~brief speculation on~~ a brief discussion of some potential causal factors of the observed correlations, including the role of aerosol in modifying atmospheric humidity and the potential implications for the understanding of aerosol effects on clouds.

Methods

In the following sections, unless otherwise stated, ~~the aerosol conditions presented have been determined by~~ aerosol conditions are determined using the aerosol number concentration ~~as~~ measured by the condensation particle counter (CPC) instrument at MCOH (Fig. 2). Other aerosol metrics used are aerosol optical depth (AOD) ~~as measured both~~ measured by the MCOH AERONET sun photometer; satellite-based AOD from the MODIS instruments on board NASA's Terra and Aqua satellites; and black carbon (BC) concentration measured by an airborne or ground-based aethalometer.

The cloud liquid water path (LWP) given here is the average-peak value (the mean of all cloud retrievals within $100\,\mathrm{g\,m^{-2}}$ of the peak cloud value) for each cloud event (Fig. 3). This definition preserves the peak LWP as a characteristic of the cloud (Warner, 1955) while accounting for instrument noise and variability within the cloud. Further discussion of identification and processing of cloud "events" is given in Appendix A1.

Three unmanned aerial vehicles (UAVs) were flown during CARDEX. MAC4, MAC5, and MAC6 flew the aerosol-radiation, water vapor flux, and cloud microphysics payloads, respectively. A more detailed description of each payload may be found in Ramanathan et al (2007); Ramana et al (2007); Corrigan et al (2008); Roberts et al (2008); Thomas et al (2012).

A complete description of the permanent MCOH instrumentation and data used in this paper has been given in Ramana and Ramanathan (2006). Additional information on the CARDEX-specific instrumentation used, including the lidar and the microwave radiometer and the methodology for processing these data, may be found in the Appendix A1.

2 Atmospheric regime as indicated by total-column water vapor content

The high variability in total-column atmospheric water vapor observed during CARDEX (~~ranging from 20–60~~between 20 and 60 $\mathrm{kg\,m^{-2}}$, Fig. 2) allows one to categorize the observations as either "wet" (here defined as total-column PWV $> 40\,\mathrm{kg\,m^{-2}}$; blue in Fig. 2) or "dry" (total-column PWV $< 40\,\mathrm{kg\,m^{-2}}$; black in Fig. 2). This distinction ~~allows insight into specific aspects of atmospheric structure in the region~~is significant in the context of later analysis (Section 3); first we describe the notable differences observed between these two regimes.

In this analysis, vapor conditions are identified primarily using the MWR total-column PWV, chosen for its high temporal resolution. Using the good agreement between the MWR and AERONET column PWV, the CARDEX flight days before MWR operations began on 6 March are additionally classified. Daily-averaged PWV conditions for the entire CARDEX period are given in Table 1, and classifications for each UAV flight are given in Table 2.

2.1 Observed distinctions between dry and wet atmospheric conditions

Table 3 shows the differences in observed MCOH surface parameters for wet vs. dry conditions ~~on~~ at one-minute resolution. There are some prominent differences between the two populations: on average, dry cases correspond to higher wind speed in both north–south and east–west directions, as well as lower surface pressures; as may be expected, the surface humidity is ~~also~~ greater for wet cases, and wet days also exhibit greater variability in cloud LWP. ~~Figures A1 and A2 illustrate the frequency distributions of parameters measured for wet vs. dry conditions.~~ There were no significant differences in observed average aerosol amount (CPC number concentration or AERONET column AOD), cloud base or boundary

layer height, or surface fluxes between the two populations when considering the variability of the observations. The frequency distributions of these parameters are visualized in Appendix Figures A1 and A2.

The vertical profiles from the MAC4 aircraft under wet (dark blue) and dry (cyan, black) conditions are shown in Fig. 4. It is first notable that in both categories, the UAV profiles indicate large variability in aerosol throughout the atmospheric column (i.e. both boundary layer aerosol and free troposphere aerosol), in terms of CPC number concentration as well as the aethalometer black carbon concentrations measured by the aircraft. Other measured values from MCOH (Fig. 4, Table 3) show only slight differences between the two populations; in particular this is true for the average LWP and surface flux values, although the variability in observed LWP is more than a factor of two larger for the wet cases. The measured cloud base heights also show greater variability under these "wet" conditions.

There is on average slightly lower boundary-layer humidity for the dry flight days compared with wet days, but the most notable difference between the two populations is in the atmospheric temperature and humidity vertical structure. While the dry days have a very well-defined boundary layer top between roughly 1000 and 1500 m, as indicated by a strong observed temperature inversion and a sharp decrease in relative humidity, the wet days do not. ~~Note that the atmospheric moisture described here is given as relative humidity (RH). For a fixed specific humidity (q), an increase in temperature would produce a decrease in RH; however, RH is used here as this is the value which was directly measured by aircraft, and this value is seen to be consistent with q values (e.g. Fig. A11).~~ Thus the most significant distinction in the atmospheric structure of the two populations is in the conditions at the top of and above the boundary layer, ~~especially~~ namely the lack of temperature inversion and greater atmospheric humidity at higher elevations for the "wet" cases. This ~~analysis~~ conclusion is additionally supported by the ECMWF reanalysis over MCOH (Appendix Fig. A3a and b).

Note that the atmospheric moisture described here is given as relative humidity (RH), as this metric was directly measured by the aircraft. Although an increase in temperature

would produce a decrease in RH for a fixed specific humidity (q), in our cases the measured RH is seen to be consistent with q calculated incorporating changes in temperature.

It is worth noting that during CARDEX, the lidar- and aircraft-measured cloud base heights were generally close in altitude to the inversion (Fig. 4). While many of these clouds likely penetrated at least partway through the top of the temperature inversion, rather than being capped by it, the strength of the observed inversion may help explain the relatively thin clouds in CARDEX as compared with previous works~~(summarized in~~ . (A summary of observations from historical trade cumulus studies may be found in Appendix Fig. A4 and Table A1~~).~~.)

2.2 Large-scale contrasts between high and low water vapor conditions

In exploring the mechanisms ~~which may contribute~~ contributing to this wet/dry distinction, we ~~analyze~~ compare the air mass back trajectories ~~as determined by~~ from the NOAA HYSPLIT model for each case (Fig. 5). ~~While~~ This analysis shows that while there is large variability in lower-level flow for both wet and dry cases, there are consistent differences in the upper-level flow of each case. On extremely dry days (Fig. 5a), the back trajectories indicate that upper-level atmospheric flow originates over the Indian subcontinent, traveling in an anticyclonic motion before arriving at MCOH as northeasterlies. During the ~~7day~~ 7-day air mass history, the air was continuously descending to the 2–3 km range. In contrast, for high-PWV conditions (Fig. 5b), upper-level air masses are easterly, approaching from the Bay of Bengal and Indonesia, and the 2–3 km air over MCOH has ascended from the boundary layer to the free troposphere within 4 days of observation. These results are consistent with the aircraft measurement results (Fig. 4): the primary distinction between wet and dry cases is in the upper-level air mass conditions~~: in~~ . In "wet" cases, this air originates from a more moist (low-level) environment and is transported aloft, while in "dry" cases it originates from a drier (upper-level) environment, and is brought to lower altitude due to strong subsidence in the atmosphere above the boundary layer. ~~A~~ The large-scale meteorological reanalysis from ECMWF ~~(Fig. A3c and d)~~ is also consistent with this interpretation, suggesting stronger subsidence and a corresponding increase in low-level divergence are present

in the dry cases ~~.~~ (Fig. A3c and d). The origin of low-level air ~~as seen in the reanalysis~~ again showed no correlation with the wet/dry distinction.

The different characteristics of wet vs. dry cases are thus primarily attributable to differences in the large-scale advection which brings air masses to MCOH, as is evident in the CARDEX observations, the air mass back trajectories, and large-scale reanalysis. This difference in origin corresponds to greater variability in the clouds formed during "wet" conditions; ~~by considering~~ when considering only the "dry" cases ~~only, we can thus better analyze the subtle correlations present in each case~~with a narrower range of variability in LWP, we are able to detect a statistically-significant correlation between aerosol and cloud variability. We hypothesize that the greater variability of LWP is a result of unconstrained vertical development of the clouds which form under more humid conditions; as greater humidity tends to increase cloud thickness, greater upper-level humidity may feed cloud development that is decoupled from boundary layer conditions. The variability within the dry cases is the focus of the following sections.

3 Characterization of observed high- vs. low-pollution conditions during CARDEX

Analysis of the meteorological conditions observed during CARDEX indicated that there was no correlation between cloud liquid water and any measured surface parameter for the CARDEX dataset as a whole. High variability is also present in the relationship between the measured cloud liquid water and surface aerosol concentration (Fig. 6a). However, when ~~filtered by PWV into "wet" vs. "dry" cases~~the data are filtered to take into account meteorology, there is a ~~statistically significant (~~positive correlation between LWP and aerosol which is significantly greater than zero (Spearman $\rho = 0.48$; Pearson $R = 0.42$, both at the 95 % confidence level) ~~increase in LWP (on a logarithmic scale) with increasing aerosol~~ for the "dry" (PWV $< 40\,\mathrm{kg\,m^{-2}}$) cases only (Fig. 6b). Note that for the Pearson correlation analysis we have taken the logarithmic transform of the LWP as these data exhibit a lognormal rather than normal distribution; the non-parametric Spearman coefficient is insensitive to the logarithmic transform. It is notable that this positive corre-

lation is ~~of opposite sign to~~ opposite the expected sign of the cloud burnoff effect, despite the presence of significant absorbing aerosol in the region~~, and is not~~ ; nor is it indicative of a constant LWP as may be expected in a traditional analysis of the first indirect effect.

~~Figure 6 shows the cloud LWP increases with increasing aerosol concentration for "dry" cases only.~~ In the following section we focus on these dry cases, which correspond to a more well-defined, structured boundary layer as described above. In this analysis, we use all low/high pollution dry days which had reanalysis and satellite data available (Table 1)~~where available (i.e. large-scale reanalysis and satellite observations)~~; observations from the UAVs are necessarily limited to the subset of these days when a UAV was flown (Table 2). "Low pollution" cases are defined as having surface CPC measurements less than $1000\,\mathrm{cm}^{-3}$ (9 flights over 5 days), and "high pollution" cases are defined as having surface CPC greater than $1500\,\mathrm{cm}^{-3}$ (17 flights over 20 days). For simplicity, in the following sections these are referred to as Case L and Case H. The "moderately polluted" cases (~~$1000 < \mathrm{CPC} < 1500$~~$1000 < \mathrm{CPC} < 1500\,\mathrm{cm}^{-3}$) are excluded from the figures in order to bring focus to the high/low pollution contrast; however, Table 4 shows that these observations consistently fall between Case L and Case H ~~,~~ (e.g. LWP, z_{PBL}, LEF), and in many cases ~~they~~ are in fact closer to Case H values ~~.~~ (e.g. LCL, z_{cb}, humidity). This holds true for the UAV vertical profiles (T, RH, aerosol) as well.

3.1 ~~Surface~~ In-situ measurements of surface and boundary layer characteristics

The summary of the mean values for each pollution case is illustrated in Fig. 7 with values given in Table 4. Frequency distributions of significant parameters are shown in Fig. 8. As expected, the more polluted dry cases show a higher average cloud LWP; these cases also correspond to lower surface wind speed and lower surface specific and relative humidities, although the total-column PWV did not show a statistically-significant difference. Perhaps most strikingly, Case H shows smaller surface latent heat flux when compared with Case L, indicating that the higher observed atmospheric humidity is not due to increased surface evaporation. While this is in large part due to the lower observed wind speed in Case H, the lower surface fluxes during high aerosol conditions may partially be a result of surface

dimming due to increased atmospheric absorption by black carbon and other absorbing aerosols (Ramanathan and Carmichael, 2008; Stanhill and Cohen, 2001; Wild, 2009) .

The UAV flight data offer further valuable insights into the possible mechanisms behind the observed ~~positive correlation between LWPand pollution~~increase in polluted LWP. Figure 9 shows the observed Case L and Case H flight profiles from the aerosol-radiation UAV~~, while Fig. A10 shows the difference between the means of Case H and Case L.~~ . Note that Case H is uniformly more polluted (as measured by both the CPC and aethalometer) through the lower atmosphere up to about 2 km, at which point average pollution decreases for both cases. This is true for all cases except for one Case L flight which sampled an elevated aerosol plume. Case H exhibits warmer temperatures throughout the atmospheric column, with the maximum mean difference between the two cases occurring around the temperature inversion/cloud layer altitude (due to systematic differences in inversion height for Case L vs. H). Note that while Figure 7 and Table 4 show that the mean temperature measured directly at the surface was not statistically different between the two categories, this is not inconsistent with the aircraft observations, which show a smaller difference between the two cases near the surface compared with higher altitudes. The more polluted cases rather uniformly have higher boundary-layer relative humidity, and substantially higher free troposphere relative humidity. ~~The slight negative values observed in the mean difference RH (H-L) (Fig. A10)~~ The brief exception to this is around 800 m~~correspond~~ , where the humidity of Case L is greater than that of Case H; this corresponds to differences in the average altitude of the sub-cloud mixed layer between the two cases, which is higher in altitude for Case L. Case H again has higher RH above the inversion, which may partly facilitate the correspondingly larger average cloud water content in this case, similar to the hypothesized mechanism behind the variability in cloud liquid water for the "wet" versus "dry" cases as discussed in Section 2, though to a lesser degree.

It is clear from these figures that higher pollution days are correlated with both higher water vapor content and higher temperatures in the entire atmospheric column, particularly around the temperature inversion ($\sim$ 800–1500 m), which is itself stronger in Case ~~H.~~

The summary of the mean values for each pollution case is illustrated in Fig. 7, and values are given in Table 4. The less polluted dry cases correspond to greater surface wind speed and lower surface specific and relative humidities (Fig. 8), although the total-column PWV did not show a statistically-significant difference. Perhaps most strikingly, Case H shows smaller surface latent heat flux when compared with Case L, indicating that the higher observed atmospheric humidity is not due to increased surface evaporation. While this is in large part due to the lower observed wind speed in Case H, the lower surface fluxes observed during increased aerosol conditions may partially be a result of surface dimming due to increased atmospheric absorption by black carbon and other absorbing aerosols (Ramanathan and Carmichael, 2008; Stanhill and Cohen, 2001; Wild, 2009) .

Figure 7 and Table 4 show that mean temperature measured directly at the surface was not statistically different between the two categories. This is not inconsistent with the aircraft observations, which show a smaller difference between the two cases near the surface compared with higher altitudes (Fig. A10). Frequency distributions of some significant parameters are shown L. The average profiles of equivalent potential temperature in Fig. 8.

The vertical structure of the atmosphere, as measured or calculated from the flight data, is further described in Fig. A11. These profiles provide 9d provide further insight into the differences in thermodynamic structure of between each case. The profiles of equivalent potential temperature show θ_e to be constant within the mixed layer, while the saturation equivalent potential temperature (θ_e^*, dashed line) decreases with height to the LCL. The layer of saturation, indicated by values of θ_e equal to those of θ_e^*, is significantly greater in vertical extent for the high pollution cases (approximately 200 m thick), whereas the low pollution profiles barely reach saturation before the temperature inversion. Above this layer is a sharp increase in θ_e^* following the inversion, coincident with a sudden decrease in θ_e due to the sudden decrease in ~~q~~ humidity at the top of the boundary layer. Note that the intersection of θ_e and θ_e^* is ~~higher~~ also lower in altitude for Case ~~L~~H, corresponding to the ~~higher~~ lower z_{cb}. The increase in θ_e^* across the boundary layer top is much greater for Case L than Case H, indicating that the high pollution cases are less stably stratified. This,

in addition to the greater latent potential energy of these more moist parcels, may result in Case H clouds more frequently achieving convection up through the temperature inversion, resulting in thicker (and thus higher LWP) clouds.

We explore the dependence of LWP on meteorological factors through a calculation of the adiabatic cloud LWC (described in more detail in Appendix A2), and conclude that an increase in LWP of the magnitude seen in the observations is likely attributable to a physical thickening of the cloud resulting from the lower cloud base; additionally, only the increased atmospheric humidity under polluted conditions, rather than increased temperature, could result in this lower z_{cb}. That cloud bases are lower for the more polluted case is further corroborated by the measured lidar cloud base heights (Fig. 8), which indicated lower average z_{cb} for highly polluted cases, and by the UAV flight data (Fig. 10), which indicated systematically lower cloud penetrations for high pollution cases. Although this is not a definitive indication that the cloud bases themselves were lower, as the plane penetrated clouds at a variety of altitudes of undetermined distance above z_{cb}, it is nonetheless consistent with lower cloud bases in Case H. While it was not possible to directly measure cloud top heights during CARDEX, ~~this interpretation is corroborated by~~ a statistical analysis of cloud tops in the region from the CALIPSO satellite (Wilcox et al, 2014), ~~which~~ found higher cloud tops associated with higher pollution levels, which also supports the conclusion of physically thicker polluted clouds.

These multiple datasets paint a consistent picture of the systematic differences between low and high pollution cases both at the surface and throughout the atmospheric column. A more polluted atmosphere is observed to be simultaneously warmer, more humid, and more convectively unstable, producing physically-thicker, higher-LWP clouds. Further examination of these conditions ~~using an idealized calculation (described in~~ (Appendix A2) indicates that only the observed changes in humidity (rather than changes in temperature) would be able to account for differences in cloud height of the magnitude of those observed between low and high pollution conditions. We now turn to a larger-scale analysis to further explore the causes of these observed correlations.

3.2 Large-scale variability between low and high pollution cases

While thus far we have ~~discussed aerosol as~~ presented aerosol in terms of the surface particle number concentration measured at the MCOH observatory, in the following large-scale analysis we use the satellite-retrieved AOD as a metric of pollution level to allow for analysis on a larger scale.

3.2.1 Regional aerosol patterns

Figure 11 (top row) shows the difference in mean MODIS AOD over the CARDEX region for the average of ~~case~~ Case (H-L) days. That is, (H-L) is taken as the mean of all high pollution (dry) days minus the mean of all low pollution (dry) days during the CARDEX period (Table 1). From left to right, the top row panels show the difference between average AOD for the 3, 2, 1, and 0 days preceding high-pollution minus low-pollution conditions (as measured at MCOH). The separate average Case L and Case H ~~AODs~~ values from Fig. 11 with overlaid 1000 hPa wind fields are shown in ~~Fig. A6~~Appendix Figures A6, A7, and A8.

It is evident from this large-scale perspective that the pollution level classifications as determined by the conditions over MCOH are not necessarily representative of the region as a whole. Indeed, the absolute values of MODIS AOD over the broader CARDEX region for the mean of all Case L days ~~indicates lower aerosol at MCOH, but~~ shows high aerosol concentrations are present elsewhere in the northern Indian Ocean at the same time as low-aerosol conditions dominate at MCOH (Fig. A6). This is particularly true over the Indian subcontinent, where (H-L) is negative (i.e. the AOD for Case L is significantly higher in magnitude than for Case H).

In Case H and in particular the (H-L) case, it is clear that the region of high AOD approaches MCOH from the north-northwest rather than the east-northeast, corresponding to the 1000 hPa wind field rather than to winds higher in the troposphere, thus indicating that lower-level transport is primarily responsible for the high pollution conditions at MCOH. Elevated plumes, which approach MCOH from the northeast, are not the major contributor to aerosol loading on these days. It is also notable that the high aerosol concentra-

tion air mass can be seen to dissipate over the 4 day period, indicating a concentrated source and subsequent dispersion of polluted air throughout the region as the plume ages. ECMWF divergence fields (Fig. A9) indicate that there is greater low-level divergence (at the 1000 hPa level) for the low-pollution cases. ~~This may contribute somewhat to dilution, but the location of the aerosol indicated by MODIS suggests that~~ Although this divergence may act to dilute the polluted air mass, the MODIS AOD shown here suggests that dilution is not the dominant factor distinguishing the two cases~~is not dilution of the aerosol mass, but rather differences in circulation which prevents the polluted air~~. Rather, polluted air is prevented from arriving at MCOH during the low pollution cases due to the differences in advection patterns.

3.2.2 Correlation between large-scale aerosol and temperature

Figure 11 (middle row) shows the (H-L) mean difference for the ECMWF 1000 hPa temperature field. Similar to the patterns in the MODIS AOD, the high temperatures in Case H are seen to be concentrated in a region which approaches MCOH from the north, and then ~~slightly~~ somewhat dissipates over the four days in question as the polluted air mass is advected southward. The remarkable spatial coincidence of temperature with the maximum AOD over all three days is strongly suggestive of heating of the air mass due to absorbing aerosol, likely occurring since before the air mass leaves the subcontinent. The rate of aerosol heating was estimated by Ramanathan et al (2007) to be on the order of 0.5 K day^{-1} for similar BC concentrations over the same region. The positive temperature anomaly is strongest at the surface; it is similar but weaker in the 900 hPa field and nonexistent at 800 hPa. ~~Temperature reanalysis for Case L and Case H overlaid by the 1000winds are shown in Fig. A7. The bottom row of Fig. 11 will be discussed in Sect. 3.3.~~

The analysis of Fig. 11 suggests that regions of high temperature are coincident with higher aerosol. We further explore this relationship with Fig. 12, which shows the correlation between AOD and T over the region. For both pollution cases, Fig. 12 shows a substantial region of statistically-significant correlation (95 % level, indicated by hatching) between AOD and T. These correlation coefficients (and those in Fig. 13) were de-

termined by calculating the Pearson correlation R ~~for each latitude/longitude point using the relationship between~~ between AOD and T for all days in question (i.e. all H days, or all L days)~~.~~, for each individual $1^\circ \times 1^\circ$ latitude/longitude point. Finally, points were only classified as "significant" if there were no more than 10% of MODIS retrievals missing. While both Case L and Case H are shown for comparison, it should be noted that due to fewer Case L days being observed (Table 1), the correlations for Case H (left panel) should be considered more robust. Analysis for all days indicates a similar pattern to Case H, although weaker in magnitude.

The region of high positive and significant correlation for Case H is present over ~~much~~ a broad extent of the Arabian Sea (the low-level source region to MCOH). The ~~AOD-T correlation is less strong in absolute magnitude for Case H, but is significant over a broader spatial extent, while~~ correlation weakens in both magnitude and area of significance between Day H-2 and Day H, which further suggests a dispersion of the polluted air mass with time, consistent with the above interpretation of Fig. 11. Case L ~~suggests a stronger correlation concentrated in a~~ shows a smaller region of ~~the Arabian Sea~~positive correlation concentrated to the north in the Arabian Sea, suggesting that while high pollution and temperature are again coincident, the polluted air mass simply is not advected in the direction of MCOH in these cases. That is, in the so-called low pollution cases (as defined by conditions at MCOH), the high-pollution, high-temperature air mass remains concentrated to the north rather than spreading – and dispersing – southward towards MCOH. Indeed, the difference between regionally-averaged AOD for the two cases over the region is only 0.05, a factor of 2–3 smaller than the maximum H-L difference. ~~The correlation weakens in both magnitude and area of significance between Day H-2 and Day H, which further suggests a dispersion of the polluted air mass in Case H. This is consistent with the above interpretation of Fig. 11.~~

The smaller region of significant negative correlation to the east of the subcontinent (particularly evident in Case H) may be explained by low atmosphere/surface dimming due to an elevated aerosol plume rather than the high boundary-layer aerosol responsible for the positive correlation to the northwest; at higher altitudes, for example

at 875 hPa ($z \approx 1250$ m), the AOD and temperature T_{875} show a strong positive correlation ~~in~~ over this region. Elevated aerosol plumes are generally seen to approach MCOH from this direction, following the upper-level wind field, consistent with the findings of ~~Höpner et al (2015)~~ Höpner et al (2016) .

3.3 Correlations between aerosol, cloud water content, and atmospheric humidity

~~Figures 6 through 8 have indicated that more polluted conditions correspond to systematically greater measured cloud liquid water and to greater boundary layer water vapor content. While not the only factor, increased water vapor may to a degree lead to increased cloud LWP. We explore this relationship through a calculation of the adiabatic cloud LWC (Appendix A2), and conclude that the observed increase in cloud LWP for increased pollution is primarily attributable to a lowering of the cloud base due to increased atmospheric humidity, rather than to changes in temperature. That cloud bases are lower for the more polluted case is further corroborated by the measured lidar cloud base heights (Fig. 8), which indicated lower average z_{cb} for highly polluted cases, and by the UAV flight data (Fig. 10), which indicated systematically lower cloud penetrations for high pollution cases. While this is not definitively an indication that the cloud bases themselves were lower, as the plane penetrated clouds at a variety of altitudes of undetermined distance above z_{cb}, it is nonetheless consistent with lower cloud bases in Case H. The atmospheric profiles of equivalent potential temperature (Fig. A11) additionally support this, indicating that under highly polluted conditions, rising air parcels reach saturation at a lower altitude and the atmosphere exhibits a thicker saturated layer compared with the low-pollution conditions, further supporting the conclusion that the atmosphere is more humid and cloud bases are lower for high pollution conditions.~~

The bottom row of Fig. 11 shows the mean (H-L) relative humidity for the larger region surrounding MCOH~~; the H and L means separately overlaid with winds are shown in Fig. A8.~~ . Again, there is a notable difference between Case H and Case L: the H-L indicates that Case H corresponds to an air mass of high RH approaching MCOH over the four days prior to the given event. However, in contrast to the ~~in contrast to the~~ top two rows, the region of

highest RH difference is seen to lag the high AOD/high temperature region by roughly one day, and develops rather than disperses with time. That is, the region of higher RH is seen to be relatively small at −3 days, and subsequently strengthens in magnitude and spatial extent ~~,~~ – approximately coincident in location with the ~~maximum~~ high AOD/temperature ~~,~~ air mass– in the time leading up to the day in question. This lagged intensification of RH over the 4 day period suggests that some effect within the polluted air mass may be acting to increase its moisture content even as the air mass disperses. This effect is not seen in higher-altitude RH fields.

The correlation between AOD and RH (Fig. 13) exhibits a similar high-low contrast to that observed in the correlations between aerosol and temperature (Fig. 12): Case H has a weaker correlation over a larger region, whereas Case L is concentrated in a smaller, more highly-correlated region. However, this relationship differs significantly from the temperature plots in that instead of dispersing in the 1–2 days prior to Case H, the correlation between AOD and RH is seen to strengthen during this period.

While not the only factor, the increased humidity shown in Figures 6 through 9 and the bottom row of Fig. 11 may to a degree contribute to the observed increase in cloud LWP. As was discussed in Section 3.1, this hypothesis is supported by calculations attributing the increase in LWP to the lowering of cloud base heights (Figs. 8 and 10) resulting from increased atmospheric humidity. The atmospheric profiles of equivalent potential temperature (Fig. 9) also indicate that under highly polluted conditions, rising air parcels reach saturation at a lower altitude and the atmosphere exhibits a thicker saturated layer compared with the low-pollution conditions, further supporting the conclusion that the atmosphere is more humid and cloud bases are lower for high pollution conditions. The large-scale picture shown by Figs. 11 and 13 indicate that, in contrast to the high temperature condition, this high humidity condition develops along with the polluted air mass, rather than exiting the continent as simultaneously warm, humid, and polluted.

The question then becomes: what may be causing this higher humidity condition to develop within a polluted air mass? We now explore some potential causal mechanisms by which aerosol may affect atmospheric humidity–and, by extension, cloud properties.

~~Discussion of potential humidification mechanisms~~

3.3.1 Discussion of potential humidification mechanisms

As shown above, there is substantial evidence of a positive correlation between observed aerosol amount and atmospheric humidity. While the present observations ~~cannot determine for certain~~ are not sufficient to determine the causal mechanism~~behind the observed correlations, we have provided evidence of correlations between aerosol and humidity. We next briefly speculate on potential mechanisms by which aerosol may affect atmospheric humidity (and thus by extension cloud properties) and present these as~~ , we are able to briefly explore some possibilities which present interesting avenues for further study.

We have previously eliminated sea surface evaporation and decreased cloud formation as the primary causes of the observed higher humidity, due to the flux and LWP measurements already described. We may additionally neglect precipitation in this case, as drizzle was not observed in these clouds even under low-pollution conditions. This leaves large-scale factors ~~,~~ (e.g. advection of warm, humid, and polluted air masses), local top-of-boundary-layer fluxes, or possible aerosol-induced effects as potential contributing factors to the observed higher relative humidity. ~~To first~~

To assess the possible influence of large-scale meteorological conditions on humidity, we ~~turn to the~~ examine HYSPLIT back trajectories ~~, which show the near-surface flow originating from the north/northwest region, with~~ for any systematic differences in the origin or evolution of the air masses for each case. These show the upper-level flow ~~under high pollution conditions in particular originating primarily from~~ approaching from the northeast over the subcontinent, consistent with the results shown in ~~Sect. 2 . Upper-level humidity also appears to increase with time for the high pollution cases even as the air is subsiding, possibly indicative of increased mixing from within the boundary layer. Low~~ Section 2 (Fig. 5b). The near-surface flow originates generally from the north/northwest for both cases; although low pollution conditions exhibit less extended back trajectories (i.e. lower wind speed above the boundary layer), ~~but~~ they come from generally the same direction.

We thus found no clear meteorological distinction (in terms of humidity level or origin) between the two cases which might explain the difference between their boundary-layer conditions. While meteorological conditions may be a potential causal factor of the observed correlation between aerosol and cloud properties (e.g. Mauger and Norris, 2007, 2010), the present observations are not sufficient to definitively establish or discard this hypothesis. Further study of the large-scale context is necessary to more fully explore the potential meteorological influences on the low/high pollution distinction and on the aerosol–humidity relationship.

~~Via aircraft and surface measurements as well as reanalysis data, we found the atmosphere to be warmer under more polluted conditions. The strong correlation between aerosol and temperature indicates that BC warming is a likely cause of this increased temperature. Taking a large-scale view, we find that the high aerosol optical depth is correlated with a high temperature over the region as a whole and in particular in the location of the air mass approaching MCOH. Simple calculations (Appendix A2) indicate that the increase in RH was the only potential factor which could account for the magnitude of the observed greater polluted cloud LWP compared with low pollution conditions, due to a lowering of the LCL and thus the cloud base height. However, the single-point observations made over MCOH are alone insufficient to establish the causal mechanism behind the observed correlations. In addition to higher temperatureunder high pollution conditions, we find that there is substantially higher atmospheric RH under polluted conditions.~~

~~For both pollution cases, there is a region of statistically-significant correlation (95level) between both AOD and T (Fig. 12), and AOD and RH (Fig. 13). While the~~ Another possible mechanism to explain the high humidity relates to the temperature/aerosol relationship. While the observed development of the AOD/T relationship (Figs. 11 and 12) is consistent with that of aerosol heating of the air mass (Ramanathan et al, 2007), there are two possible interpretations of ~~the strengthening pattern in the correlation in Figs. 11, 12, and 13: first, aerosol conditions may be directly or indirectly increasing the boundary layer humidity , or second,~~ how this may relate to the development of high humidity conditions. First,

the humidification of the boundary layer may ~~result from~~ be a result of the meteorological history of the air mass coincident with aerosol conditions (e.g. Mauger and Norris, 2007)~~. For the first possibility, aerosol heating of the more polluted air mass may be driving mesoscale circulation to bring moisture to the more polluted region. Alternately~~; second, aerosol conditions may be directly or indirectly increasing the boundary layer humidity. As shown above, the first interpretation is not supported by the present study, though a more complete analysis is necessary. Regarding the second possibility, aerosol heating may suppress turbulent mixing and stabilize the boundary layer, lowering BL height and ~~thus induce~~ inducing higher relative humidity as the polluted plume ages. ~~However,~~ Alternately, the presence of aerosol heating within the more polluted air mass may be altering the mesoscale circulation to bring more moist air to the region. Again, further study is needed ~~in order~~ to establish the plausibility of these potential causal mechanisms, and ~~whether meterological~~ to determine whether meteorological or aerosol mechanisms may be primarily responsible for the observed correlations. ~~Such correlations, and the potential mechanisms behind them, should~~ Regardless of their mechanism, these correlations must be considered in such studies of aerosol–cloud interactions, as secondary changes in atmospheric properties – either directly by aerosol effects or coincident with high-pollution conditions – may alter the effective magnitude of indirect effects. As one example, the ~~so-called first aerosol indirect effect (cloud albedo effect)~~ first indirect effect relies on the assumption that the amount of liquid water in a cloud is unchanged for clean vs. aerosol-perturbed cases. As cloud albedo is a direct function of cloud liquid water, any coincident changes observed in cloud liquid water content should be considered as this may alter the expected magnitude of the aerosol-induced cloud-albedo effect. ~~The further exploration of the correlations observed here offer an intriguing avenue for~~ These observed correlations require further exploration in future research.

4 Conclusions

Here we have presented new results on the characterization of trade cumulus clouds and the dry season cloud climatology in the northern Indian Ocean using combined ground station observations, vertical atmospheric profiles from UAVs, and large-scale satellite data and meteorological reanalysis. We describe the general characteristics of the atmosphere in the region and illustrate the existence of two separate climatologies based on the water vapor ~~characteristics of the vertical profile~~conditions in the atmospheric column, which result in different populations of clouds forming~~under each~~: "dry" conditions result in clouds which tend to be constrained by a well-defined boundary layer topped by an inversion, whereas the clouds forming under "wet" conditions exhibit more unconstrained and varied development fed by the availability of more humid upper-layer air. When the data are ~~filtered~~ analyzed according to this climatological separation to ~~account for~~ filter out the large natural variability of high-vapor conditions, we observe a distinct positive correlation between ~~the~~ aerosol concentration and cloud liquid water. ~~In describing the systematic differences between low and high pollution conditions both from station data and from a large-scale perspective, we observe highly polluted conditions~~ Highly polluted conditions (with a high concentration of absorbing aerosol) are found to be systematically warmer and more humid~~.~~ ~~From~~ , as seen by the ground, aircraft, and large-scale analyses. From the in-situ aircraft and remote-sensed ground observations, we ~~observed the~~ observe a lower boundary layer height under polluted cases~~to be lower~~, resulting in a lower cloud base which is responsible for the greater cloud liquid water. The observed increase in RH was the only potential factor which could account for the magnitude of the observed difference in cloud LWP which results from this lower cloud base. The large-scale analysis indicates that highly polluted air masses exiting the subcontinent are also warmer initially, while high-humidity conditions develop along with the air mass as it ages.

~~The CARDEX results show that high-aerosol conditions (corresponding to a high concentration of absorbing aerosol) are consistently warmer, and also tend to be systematically wetter than less-polluted cases; while the higher temperatures may be~~ While

the strong correlation between aerosol and temperature is likely attributable to aerosol heating of the air mass (e.g. Ramanathan et al, 2007), with the given observations we are unable to definitively determine a causal mechanism ~~to the observed aerosol–humidity correlation . We have offered some brief discussion of possible~~ responsible for the observed correlation between aerosol and humidity. Possible mechanisms which may be ~~at play, including~~ producing these correlations include meteorological or aerosol-driven ~~humidification (~~factors, though we were not able to attribute the observed differences to differences in large-scale advection patterns. There remains the possibility that aerosol effects may be driving the observed lagged humidification of the boundary layer, either by influencing the mesoscale circulation or stabilizing the boundary layer locally~~), or meteorological conditions coincident to the higher aerosol conditions.~~ ; this is an intriguing avenue for further study.

Understanding the consequences of aerosol–cloud interactions in this region requires an understanding of how variations in atmospheric conditions such as temperature and humidity may impact cloud dynamics and water content. Additionally, future research aiming at understanding aerosol–cloud interactions as a whole, and effects of aerosols influencing atmospheric dynamics specifically, should incorporate both local observations of the instantaneous vertical structure and motion of the atmosphere, as well as large-scale observations to understand the air mass history and the potential influence of meteorology on these effects.

Appendix A:

A1 Extended Methods

The microwave radiometer (MWR) used during CARDEX was on loan from the Department of Energy's Atmospheric Radiation Measurement (ARM) Climate Research Facility. As described in the instrument's documentation (Morris, 2006), the MWR passively collects microwave radiation at two wavelength bands centered at 23.8 and 31.4 GHz, chosen to cor-

respond to predominantly water vapor and liquid water emission, respectively. MWR LWP values were flagged as cloud retrievals if they were more than 35 g m^{-2} above a 1000-point running mean, a value chosen to reflect the instrument noise level and retrieval uncertainty. Two or more consecutive cloud-flagged retrievals are collectively considered a "cloud event" (Fig. 3, inset). An absolute maximum of 130 g m^{-2} was imposed on the running mean to avoid obvious cloud retrievals skewing the background mean. These values were empirically determined to maximize the number of clouds identified while discounting spurious "cloud events" that were a product of noise in the instrument. To this end, "cloud events" are defined as having two or more consecutive cloud-flagged retrievals; all single-retrieval "events" were excluded from analysis.

The mini-micropulse lidar (MPL) retrievals consisted of vertically-resolved backscatter data at 30 m resolution above 250 m, collected at 0.1 Hz. The MPL was operated daily between 22 February and 30 March for as many hours as was permitted by ambient operating conditions. Completely continuous operation was not possible due to the sensitivity of the instrument to conditions of heat, direct sunlight, and ambient humidity, which required constant operator supervision. The instrument was also switched off around noon particularly as the equinox approached to avoid direct overhead solar glare into the instrument cavity. The MPL was successfully operated for four overnight periods, on 20 and 22–24 March, to fully characterize the diurnal cycle.

Individual UAV flights were classified as "wet" or "dry" by taking the average PWV for $\pm$2 h around the flight time. During CARDEX, the MAC4 aircraft had 12 flights during dry conditions and 5 during wet conditions; the MAC5 aircraft had 15 dry and 4 wet flights; and MAC6 had 10 dry and 4 wet flights. We examine the different aircraft individually due to the differences in flight patterns, with a focus on the MAC4 (aerosol and radiation payload) data in the context of thermodynamic profiling, as this aircraft most frequently profiled the entire lower boundary layer in a systematic (spiral ascending) pattern.

The parameters shown in Fig. 7 and Table 4 were calculated based on all minute-averaged surface data except for number of cloud events, cloud LWP, and the cloud base height, which are the averages of the cloud events occurring under the given conditions, and

latent energy fluxes, which are the averages of values measured between 6 a.m.–6 p.m. MVT due to limitations in the eddy covariance retrievals. The MCOH values obtained by averaging over just cloudy times are not substantially different from those in Table 4.

The air mass back trajectories are from the National Oceanic and Atmospheric Administration's HYbrid Single-Particle Lagrangian Integrated Trajectory (NOAA HYSPLIT) model, initialized with NCEP/NCAR reanalysis meteorology (available at http://ready.arl.noaa.gov/HYSPLIT SUBSCRIPTNBtraj.php) (Draxler and Rolph, 2013) . The large-scale reanalysis used is the European Center for Medium-range Weather Forecasts (ECMWF) ERA-Interim product (available at http://www.ecmwf.int/research/era/do/get/Reanalysis SUBSCRIPTNBECMWF) which provides large-scale meteorological parameters including vertical velocity, atmospheric convergence, wind fields, temperature, and humidity at 6-hourly, $1^\circ \times 1^\circ$ horizontal, and 25 hPa vertical resolution. Unless otherwise noted, the ECMWF time shown is the 0600Z reanalysis (1100 MVT), chosen to be closest to the overpass times of the satellites used as well as typical UAV flight times. The large-scale aerosol optical depths (AOD) shown are the NASA MODIS (MODerate resolution Imaging Spectroradiometer) $1^\circ \times 1^\circ$ daily gridded Terra and Aqua land and ocean composite AOD at 550nm, from Collection 5.1 (available at http://modis-atmos.gsfc.nasa.gov/MOD04 SUBSCRIPTNBL2/index.html).

A2 Calculations of cloud height and adiabatic cloud liquid water content

In this section we perform calculations for some idealized hypothetical scenarios to better understand the potential mechanisms behind the observations.

To explore potential causal factors relating to measured cloud liquid water, it is beneficial to explore the relative sensitivity of the LCL (and thus cloud base height) to temperature and relative humidity variability. A simple calculation following Lawrence (2005) indicates that the LCL height z_{LCL} can be approximated from surface temperature and humidity by

the following formula:

$$z_{\mathrm{LCL}} \approx \left(20 + \frac{T}{5}\right)(100 - \mathrm{RH}) \tag{A1}$$

This calculation indicates that for a constant RH, a change in temperature equal to the extremes of the ranges observed only changes the z_{LCL} by 24 m, whereas for the extremes in observed RH with a constant T, this effect can change the z_{LCL} by over 500 m. Using the mean values of Case L and Case H ($T_{\mathrm{L}} = 28^{\circ}$C, $\mathrm{RH_L} = 70\,\%$ and $T_{\mathrm{H}} = 29^{\circ}$C, $\mathrm{RH_H} = 77\,\%$), changes solely in RH between L and H are found to lower the lifting condensation level by 200 m, consistent with observed differences in z_{LCL}. This compares with a change of approximately 5 m resulting from a temperature change only. Thus the LCL is primarily determined by changes in RH. Note that the calculated z_{LCL} is 200–300 m lower than the z_{cb} indicated by the MPL; as surface air parcels ascend towards the LCL, they will mix with drier, cooler surrounding air, a factor which will raise cloud base height but is not accounted for in this idealized calculation.

Using the above result, we take changing the cloud base height to be a proxy for the effect of changing atmospheric RH.

We explore the magnitude of each effect (changing temperature vs. changing relative humidity) on the resulting cloud by calculating adiabatic cloud LWP for clouds of varying thicknesses and heights using values observed in CARDEX (Fig. A5; Table A2). While trade cumulus in particular have been observed to be significantly (60–90 %) subadiabatic (Curry and Webster, 1999; Warner, 1955), with subadiabaticity increasing with cloud thickness, a calculation of the adiabatic liquid water provides a useful metric to diagnose the relative magnitude of a given change on the cloud liquid water content.

Table A2 and Fig. A5 indicate the magnitude of each effect (i.e. independently varying the relative humidity and temperature observed in cases H and L) on the cloud liquid water content. Temperature is taken to be the measured mean values T_{L} and T_{H} as shown in Fig. A5. For RH, z_{LCL} is taken as a proxy for z_{cb}; for this idealized experiment, the heights $z_{\mathrm{LCL,L}}$ and $z_{\mathrm{LCL,H}}$ are approximated at 800 and 600 m, a difference approximately equal to the observed $\Delta z_{\mathrm{LCL,(H-L)}}$. In-cloud lapse rates are assumed to be constant at $-5.5\,\mathrm{K\,km^{-1}}$.

For a cloud of fixed thickness, lowering the cloud base z_{cb} along the same temperature profile and raising the cloud base temperature for a fixed z_{cb} have roughly the same effect on cloud LWP: an increase of 17 and 22 g m^{-2}, respectively. Both of these changes are effectively negligible given the much larger magnitude of the observed H-L LWP differences we seek to explain. We additionally note that a physical thickening of the cloud due to higher cloud tops would have a similar effect, although the magnitude is somewhat smaller: for a 500 m thick cloud with cloud base at 800 m, the LWP would be 484 g m^{-2}, for an increase of 306 g m^{-2} over the base case. However, the observations suggest that a lowering of the cloud base is at least a significant contributing factor to the cloud thickening (e.g. Figs. 8, ~~10, A11).~~ 9, and 10).

Thus for clouds of similar thickness, we find that the higher temperature or relative humidity alone cannot explain the higher observed cloud water contents of Case H. However, for a lowering of the cloud base while holding cloud top constant (i.e. thicker clouds), the adiabatic LWC is found to increase by 350 g m^{-2}. Accounting for average subadiabaticity, this difference is still $\sim$ 200 g m^{-2}.

Acknowledgements. The CARDEX field campaign was sponsored and funded by the National Science Foundation Grant ATM07-21142 and conducted by the Scripps Institution of Oceanography at the University of California at San Diego in collaboration with the Desert Research Institute, Stockholm University, Argonne National Laboratory, and the Max Planck Institute for Chemistry. V. Ramanathan is the principal investigator of CARDEX, E. Wilcox is the Co-PI and H. Nguyen was the field director who conducted the campaign with full support by the government of Maldives. We also thank the Department of Energy Atmospheric Radiation Measurement (ARM) Program for use of the microwave radiometer as well as helpful technical advice. Full details of the CARDEX campaign can be found in: http://www-ramanathan.ucsd.edu/files/CARDEX_prop_Jun_20.pdf. This study is Paper #3 from the CARDEX campaign.

References

Albrecht B (1989) Aerosols, Cloud Microphysics, and Fractional Cloudiness. Science 245(4923):1227–1230, doi:10.1126/science.245.4923.1227

Augstein E, Schmidt H, Ostapoff F (1974) The vertical structure of the atmospheric planetary boundary layer in undisturbed trade winds over the atlantic ocean. Boundary-Layer Meteorology pp 129–150

Betts A (1997) Chapter 4 The Physics and Parameterization of Moist Atmospheric Convection. In: Smith RK (ed) Trade Cumulus: Observations and Modeling, NATO ASI Series C: Vol. 505, Kluwer Academic Publishers, Dordrecht, 498pp., pp 99–126

Corrigan CE, Roberts GC, Ramana MV, Kim D, Ramanathan V (2008) Capturing vertical profiles of aerosols and black carbon over the Indian Ocean using autonomous unmanned aerial vehicles. Atmospheric Chemistry and Physics 8(3):737–747

Curry JA, Webster PJ (1999) Thermodynamics of Atmospheres and Oceans. Academic Press

Draxler R, Rolph G (2013) Hysplit (hybrid single-particle lagrangian integrated trajectory) model access via noaa arl ready website (http://www.arl.noaa.gov/hysplit.php). NOAA Air Resources Laboratory, College Park, MD

French J, Vali G, Kelly R (2000) Observations of microphysics pertaining to the development of drizzle in warm, shallow cumulus clouds. Quarterly Journal of the Royal Meteorological Society 126(563, B):415–443, doi:10.1256/smsqj.56303

Garstang M, Betts A (1974) Review of Tropical Boundary-Layer and Cumulus Convection - Structure, Parameterization, and Modeling. Bulletin of the American Meteorological Society 55(10):1195–1205, doi:10.1175/1520-0477(1974)055<1195:AROTTB>2.0.CO;2

Heymsfield A, McFarquhar G (2001) Microphysics of INDOEX clean and polluted trade cumulus clouds. Journal of Geophysical Research-Atmospheres 106(D22):28,653–28,673, doi:10.1029/2000JD900776

Höpner F, Bender FAM, Ekman AML, Praveen PS, Bosch C, Ogren JA, Andersson A, Gustafsson Ö, Ramanathan V (2016) Vertical profiles of optical and microphysical particle properties above the northern indian ocean during cardex 2012. Atmospheric Chemistry and Physics 16(2):1045–1064, doi:10.5194/acp-16-1045-2016, http://www.atmos-chem-phys.net/16/1045/2016/

Höpner F, Bender FAM, Ekman A, Praveen P, Bosch C, Ogren J, Andersson A, Gustafsson Ö, Ramanathan V (2015) Vertical profiles of optical and microphysical particle properties above the northern Indian Ocean during CARDEX 2012. Atmospheric Chemistry and Physics Discussion 15:3907–3953, doi:10.5194/acpd-15-3907-2015

Koch D, Del Genio AD (2010) Black carbon semi-direct effects on cloud cover: review and synthesis. Atmospheric Chemistry and Physics 10(16):7685–7696, doi:10.5194/acp-10-7685-2010

LaMontagne R, Telford J (1983) Cloud Top Mixing in Small Cumuli. Journal of the Atmospheric Sciences 40(9):2148–2156, doi:10.1175/1520-0469(1983)040<2148:CTMISC>2.0.CO;2

Lawrence M (2005) The relationship between relative humidity and the dewpoint temperature in moist air - A simple conversion and applications. Bulletin of the American Meteorological Society 86(2):225+, doi:10.1175/BAMS-86-2-225

Lawrence MG, Lelieveld J (2010) Atmospheric pollutant outflow from southern Asia: a review. Atmospheric Chemistry and Physics 10(22):11,017–11,096, doi:10.5194/acp-10-11017-2010

MacPherson J, Isaac G (1977) Turbulent Characteristics of Some Canadian Cumulus Clouds. Journal of Applied Meteorology 16(1):81–90, doi:10.1175/1520-0450(1977)016<0081:TCOSCC>2.0.CO;2

Malkus JS (1956) Marine meteorology: On the structure of trade-wind air below cloud. Technical Report #40: Unpublished Manuscript 56-52, Woods Hole Oceanographic Institution, doi:10.1575/1912/5433

Malkus JS (1957) Marine meteorology: On the structure of the trade wind moist layer. Technical Report #42: Unpublished Manuscript 57-9, Woods Hole Oceanographic Institution, doi:10.1575/1912/5443

Mauger GS, Norris JR (2007) Meteorological bias in satellite estimates of aerosol-cloud relationships. Geophys Res Lett 34(16), doi:10.1029/2007GL029952

Mauger GS, Norris JR (2010) Assessing the Impact of Meteorological History on Subtropical Cloud Fraction. J Climate 23(), doi:10.1175/2010JCLI3272.1

Morris VR (2006) Microwave Radiometer Handbook. Atmospheric Radiation Measurement Climate Research Facility, U.S. Department of Energy

Ramana MV, Ramanathan V (2006) Abrupt transition from natural to anthropogenic aerosol radiative forcing: Observations at the ABC-Maldives Climate Observatory. Journal of Geophysical Research-Atmospheres 111(D20), doi:10.1029/2006JD007063

Ramana MV, Ramanathan V, Kim D, Roberts GC, Corrigan CE (2007) Albedo, atmospheric solar absorption and heating rate measurements with stacked UAVs. Q J R Meteorol Soc 133(629, Part b):1913–1931, doi:10.1002/qj.172

Ramanathan V, Carmichael G (2008) Global and regional climate changes due to black carbon. Nature Geoscience 1(4):221–227, doi:10.1038/ngeo156

Ramanathan V, Crutzen P, Lelieveld J, Mitra A, Althausen D, Anderson J, Andreae M, Cantrell W, Cass G, Chung C, Clarke A, Coakley J, Collins W, Conant W, Dulac F, Heintzenberg J, Heymsfield A, Holben B, Howell S, Hudson J, Jayaraman A, Kiehl J, Krishnamurti T, Lubin D, McFarquhar G,

Novakov T, Ogren J, Podgorny I, Prather K, Priestley K, Prospero J, Quinn P, Rajeev K, Rasch P, Rupert S, Sadourny R, Satheesh S, Shaw G, Sheridan P, Valero F (2001) Indian Ocean Experiment: An integrated analysis of the climate forcing and effects of the great Indo-Asian haze. J Geophys Res-Atmos 106(D22):28,371–28,398, doi:10.1029/2001JD900133

Ramanathan V, Ramana MV, Roberts G, Kim D, Corrigan C, Chung C, Winker D (2007) Warming trends in Asia amplified by brown cloud solar absorption. Nature 448(7153):575–U5, doi:10.1038/nature06019

Roberts GC, Ramana MV, Corrigan C, Kim D, Ramanathan V (2008) Simultaneous observations of aerosol-cloud-albedo interactions with three stacked unmanned aerial vehicles. Proceedings of the National Academy of Sciences of the United States of America 105(21):7370–7375, doi:10.1073/pnas.0710308105

Rodts S, Duynkerke P, Jonker H (2003) Size distributions and dynamical properties of shallow cumulus clouds from aircraft observations and satellite data. Journal of the Atmospheric Sciences 60(16):1895–1912, doi:10.1175/1520-0469(2003)060<1895:SDADPO>2.0.CO;2

Simpson J, Dennis AS (1972) Cumulus clouds and their modification. NOAA Technical Memorandum ERL OD-14, National Oceanic and Atmospheric Administration

Stanhill G, Cohen S (2001) Global dimming: a review of the evidence for a widespread and significant reduction in global radiation with discussion of its probable causes and possible agricultural consequences. Agricultural and Forest Meteorology 107(4):255–278, doi:10.1016/S0168-1923(00)00241-0

Stevens B, Feingold G (2009) Untangling aerosol effects on clouds and precipitation in a buffered system. Nature 461(7264):607–613, doi:10.1038/nature08281

Thomas RM, Praveen P, Wilcox EM, Pistone K, Bender F, Ramanathan V (2012) First uav measurements of entrainment layer fluxes with coupled cloud property measurements. In: American Geophysical Union

Twomey S (1974) Pollution and Planetary Albedo. Atmospheric Environment 8(12):1251–1256, doi:10.1016/0004-6981(74)90004-3

Warner J (1955) The Water Content of Cumuliform Cloud. Tellus 7(4):449–457

Wilcox EM, Thomas RM, Praveen P, Pistone K, Bender F, Feng Y, Ramanathan V (2014) Shallow cumulus clouds embedded in a deep regional haze: Results from indian ocean cardex experiment. In: American Meteorological Society

Wild M (2009) Global dimming and brightening: A review. Journal of Geophysical Research-Atmospheres 114, doi:10.1029/2008JD011470

Augstein, E., Schmidt, H., and Ostapoff, F.: The Vertical Structure of the Atmospheric Planetary Boundary Layer in Undisturbed Trade Winds over the Atlantic Ocean, Bound.-Lay. Meteorol., 6, 129–150, 1974.

Betts, A.: The physics and parameterization of moist atmospheric convection, chapter 4, in: Trade Cumulus: Observations and Modeling, edited by: Smith, R. K., NATO ASI Series C, vol. 505, Kluwer Academic Publishers, Dordrecht, 99–126, 498 pp., 1997.

Corrigan, C. E., Roberts, G. C., Ramana, M. V., Kim, D., and Ramanathan, V.: Capturing vertical profiles of aerosols and black carbon over the Indian Ocean using autonomous unmanned aerial vehicles, Atmos. Chem. Phys., 8, 737–747, doi:, 2008.

Curry, J. A. and Webster, P. J.: Thermodynamics of Atmospheres and Oceans, Academic Press, San Diego, 238–239, 1999.

French, J., Vali, G., and Kelly, R.: Observations of microphysics pertaining to the development of drizzle in warm, shallow cumulus clouds, Q. J. Roy. Meteor. Soc., 126, 415–443, doi:, 2000.

Garstang, M. and Betts, A.: Review of tropical boundary-layer and cumulus convection – structure, parameterization, and modeling, B. Am. Meteorol. Soc., 55, 1195–1205, doi:, 1974.

Heymsfield, A. and McFarquhar, G.: Microphysics of INDOEX clean and polluted trade cumulus clouds, J. Geophys. Res.-Atmos., 106, 28653–28673, doi:, 2001.

Hpner, F., Bender, F. A.-M., Ekman, A. M. L., Praveen, P. S., Bosch, C., Ogren, J. A., Andersson, A., Gustafsson, ., and Ramanathan, V.: Vertical profiles of optical and microphysical particle properties above the northern Indian Ocean during CARDEX 2012, Atmos. Chem. Phys. Discuss., 15, 3907–3953, doi:, 2015.

LaMontagne, R. and Telford, J.: Cloud top mixing in small cumuli, J. Atmos. Sci., 40, 2148–2156, doi:, 1983.

Lawrence, M.: The relationship between relative humidity and the dewpoint temperature in moist air – a simple conversion and applications, B. Am. Meteorol. Soc., 86, 225–233, doi:, 2005.

Lawrence, M. G. and Lelieveld, J.: Atmospheric pollutant outflow from southern Asia: a review, Atmos. Chem. Phys., 10, 11017–11096, doi:, 2010.

MacPherson, J. and Isaac, G.: Turbulent Characteristics of Some Canadian Cumulus Clouds, J. Appl. Meteorol., 16, 81–90, doi:, 1977.

Malkus, J. S.: Marine Meteorology: On the structure of trade-wind air below cloud, Technical Report 40: Unpublished Manuscript 56-52, Woods Hole Oceanographic Institution, doi:, 1956.

Malkus, J. S.: Marine Meteorology: On the structure of the trade wind moist layer, Technical Report 42: Unpublished Manuscript 57-9, Woods Hole Oceanographic Institution, doi:, 1957.

Mauger, G. S. and Norris, J. R.: Meteorological bias in satellite estimates of aerosol–cloud relationships, Geophys. Res. Lett., 34, L16824, doi:, 2007.

Mauger, G. S. and Norris, J. R.: Assessing the impact of meteorological history on subtropical cloud fraction, J. Climate, 23, 2926–2940, doi:, 2010.

Morris, V. R.: Microwave Radiometer Handbook, Atmospheric Radiation Measurement Climatic Research Facility, US Department of Energy, ARM TR-016, 2006.

Ramana, M. V. and Ramanathan, V.: Abrupt transition from natural to anthropogenic aerosol radiative forcing: observations at the ABC-Maldives Climate Observatory, J. Geophys. Res.-Atmos., 111, D20207, doi:, 2006.

Ramana, M. V., Ramanathan, V., Kim, D., Roberts, G. C., and Corrigan, C. E.: Albedo, atmospheric solar absorption and heating rate measurements with stacked UAVs, Q. J. Roy. Meteor. Soc., 133, 1913–1931, doi:, 2007.

Ramanathan, V. and Carmichael, G.: Global and regional climate changes due to black carbon, Nat. Geosci., 1, 221–227, doi:, 2008.

Ramanathan, V., Crutzen, P., Lelieveld, J., Mitra, A., Althausen, D., Anderson, J., Andreae, M., Cantrell, W., Cass, G., Chung, C., Clarke, A., Coakley, J., Collins, W., Conant, W., Dulac, F., Heintzenberg, J., Heymsfield, A., Holben, B., Howell, S., Hudson, J., Jayaraman, A., Kiehl, J., Krishnamurti, T., Lubin, D., McFarquhar, G., Novakov, T., Ogren, J., Podgorny, I., Prather, K., Priestley, K., Prospero, J., Quinn, P., Rajeev, K., Rasch, P.,

Rupert, S., Sadourny, R., Satheesh, S., Shaw, G., Sheridan, P., and Valero, F.: Indian Ocean Experiment: an integrated analysis of the climate forcing and effects of the great Indo-Asian haze, J. Geophys. Res.-Atmos., 106, 28371–28398, doi:, 2001.

Ramanathan, V., Ramana, M. V., Roberts, G., Kim, D., Corrigan, C., Chung, C., and Winker, D.: Warming trends in Asia amplified by brown cloud solar absorption, Nature, 448, 575–578, doi:, 2007.

Roberts, G. C., Ramana, M. V., Corrigan, C., Kim, D., and Ramanathan, V.: Simultaneous observations of aerosol–cloud–albedo interactions with three stacked unmanned aerial vehicles, P. Natl. Acad. Sci. USA, 105, 7370–7375, doi:, 2008.

Rodts, S., Duynkerke, P., and Jonker, H.: Size distributions and dynamical properties of shallow cumulus clouds from aircraft observations and satellite data, J. Atmos. Sci., 60, 1895–1912, doi:, 2003.

Simpson, J. and Dennis, A. S.: Cumulus Clouds and their Modification, NOAA Technical Memorandum ERL OD-14, National Oceanic and Atmospheric Administration, 1972.

Stanhill, G., and Cohen, S.: Global dimming: a review of the evidence for a widespread and significant reduction in global radiation with discussion of its probable causes and possible agricultural consequences, Agr. Forest Meteorol., 107, 255–278, doi:, 2001.

Thomas, R. M., Praveen, P., Wilcox, E. M., Pistone, K., Bender, F., and Ramanathan, V.: First UAV Measurements of Entrainment Layer Fluxes with Coupled Cloud Property Measurements, American Geophysical Union, American Geophysical Union, Fall Meeting 2012, abstract A53G-0211, 2012.

Warner, J.: The water content of cumuliform cloud, Tellus, 7, 449–457, 1955.

Wilcox, E. M., Thomas, R. M., Praveen, P., Pistone, K., Bender, F., Feng, Y., and Ramanathan, V.: Shallow Cumulus Clouds Embedded in a Deep Regional Haze: Results from Indian Ocean CARDEX Experiment, American Meteorological Society, American Meteorological Society 94th Annual Meeting, Paper 239815, 2014.

Wild, M.: Global dimming and brightening: a review, J. Geophys. Res.-Atmos., 114, D00D16, doi:, 2009.

Table 1. Daily-averaged aerosol and water vapor conditions during CARDEX, indicating days of low (CPC $< 1000\,\mathrm{cm}^{-3}$), high (CPC $> 1500\,\mathrm{cm}^{-3}$), or intermediate/transitioning pollution conditions ($1000 <$ CPC $< 1500\,\mathrm{cm}^{-3}$). A "dry" classification indicates that total-column precipitable water vapor was less than 40 $\mathrm{kg\,m}^{-2}$, and "wet" indicates PWV greater than 40 $\mathrm{kg\,m}^{-2}$. "Borderline/transition" indicates that the daily average was within $40 \pm 1\,\mathrm{kg\,m}^{-2}$, or that the PWV shifted significantly between "dry" or "wet" conditions over the course of the 24 h period (midnight to midnight, MVT). There were 30 dry and 8 wet days during this period, corresponding to 37 dry- and 13 wet-condition flights. Flights on "borderline/transition" days may still be classified as "wet" or "dry" based on average values measured around the flight time (Table 2). Note that no water vapor data was available on 28 February, though it seems likely to be "wet" given the conditions of the previous and following days. All flights are visualized in Fig. 2.

Water Vapor	Aerosol	Dates
wet	low pollution	16–17 March
wet	middle/transition	13–15, 29 March
wet	high pollution	27, (28), 29 February
dry	low pollution	4–6, 10–11 March
dry	middle/transition	7, 9, 22–24 March
dry	high pollution	16–26 February; 2–3, 8, 19–21, 25–27 March
borderline/transition	low pollution	12 March
borderline/transition	middle/transition	18 March
borderline/transition	high pollution	1, 28 March

Table 2. CARDEX flights and corresponding surface CPC and total-column PWV conditions for the aerosol/radiation (MAC4), flux (MAC5), and cloud microphysics (MAC6) planes, indicating high (H) or low (L) pollution, and wet (W) or dry (D) total-column water vapor conditions. Conditions are determined by ± 2 hourly averages around the flight time, except for PWV before 5 March, which is determined by average AERONET-retrieved PWV. Note that there was no AERONET retrieval on 28 February and the CPC had a loss of data on 24 March (although the longer time series suggests a middle-level aerosol amount during the missing period).

Date	MAC4		MAC5		MAC6	
	Flight Time		Flight Time		Flight Time	
23 Feb	12:30	H,D				
24 Feb			12:51	H,D		
27 Feb	10:00	H,W				
28 Feb	09:00	H,N/A	14:56	H,N/A	12:00	H,N/A
29 Feb			14:53	H,W	09:30	H,W
02 Mar	08:30	H,D	13:29	H,D		
03 Mar	12:36	H,D	10:55	H,D		
04 Mar	12:30	L,D	09:03	L,D		
09 Mar					07:00	M,D
					12:00	M,D
10 Mar	10:30	L,D	13:22	L,D	08:30	L,D
11 Mar	09:45	L,D	13:09	L,D	14:30	L,D
			17:27	L,D		
13 Mar	15:15	M,W	10:14	M,W		
14 Mar	12:03	M,W			08:30	M,W
15 Mar	13:30	M,W	10:47	M,W	15:30	M,W
			17:07	M,W		
17 Mar	12:00	M,W				
18 Mar			13:59	M,D	11:00	M,D
19 Mar			15:51	H,D	11:00	H,D
					15:30	H,D
20 Mar	14:30	H,D	12:23	H,D	09:45	H,D
					14:30	H,D
21 Mar	13:30	M,D	14:18	M,D		
23 Mar	08:30	M,D	12:58	M,D	08:30	M,W
24 Mar	09:00	(M),D	13:32	(M),D		
25 Mar	09:30	H,D	14:02	H,D	12:00	H,D
26 Mar	09:23	M,D	12:45	H,D		

Table 3. Average surface values, standard deviations, and 10th and 90th percentile ranges observed for wet vs. dry conditions during CARDEX. Note the highly non-normal distributions of many of these parameters. With the exception of LEF and cloud values, these are calculated from the minute-averaged values for which PWV $< 40\,\mathrm{kg\,m^{-2}}$ or PWV $> 40\,\mathrm{kg\,m^{-2}}$. LWP and cloud base height are the more meaningful averages over cloud events only; boundary layer height additionally follows this definition to illustrate the position of cloud relative to the boundary layer. ~~Due to the low nighttime wind speeds~~Eddy covariance calculations require a 30-minute averaging period; additionally, eddy covariance fluxes were unresolvable ~~; thus~~ during nighttime due to the low wind speeds. Thus the values of LEF below are for 30-minute-averaged daytime fluxes (6 a.m.–6 p.m. MVT) only. The corresponding 24 h values are 74.8 ± 54.3 (6.0–137.3) and 67.6 ± 64.1 (3.4–133.7) $\mathrm{W\,m^{-2}}$ for dry and wet conditions, respectively. Lifting condensation level is calculated from the approximation given in Lawrence (2005).

	dry conditions (PWV $< 40\,\mathrm{kg\,m^{-2}}$)			wet conditions (PWV $> 40\,\mathrm{kg\,m^{-2}}$)		
	mean	1σ	10–90 %iles	mean	1σ	10–90 %iles
Number of cloud events	267			363		
Cloud LWP ($\mathrm{g\,m^{-2}}$)	147.0	105.3	96.3–187.2	204.2	271.4	79.9–435.2
PWV ($\mathrm{kg\,m^{-2}}$)	31.4	4.6	25.0–37.9	47.8	5.5	41.0–56.5
CPC ($\mathrm{cm^{-3}}$)	1360	352	789–1797	1218	338	778–1621
$\mathrm{AOD_{500}}$	0.48	0.17	0.26–0.66	0.43	0.23	0.20–0.73
Wind speed ($\mathrm{m\,s^{-1}}$)	2.2	1.2	0.8–4.0	1.6	0.9	0.6–2.8
Surface temperature (°C)	28.6	1.0	27.4–30.1	28.8	1.1	27.5–30.4
Surface pressure (hPa)	1008.2	1.9	1005.6–1010.7	1009.4	1.5	1007.4–1011.6
Relative humidity (%)	75.6	5.3	68.5–82.3	77.9	4.8	71.7–84.2
Specific humidity ($\mathrm{g\,kg^{-1}}$)	18.5	1.3	16.3–20.1	19.2	0.9	18.1–20.1
Boundary layer height (m)	895	193	674–1109	841	163	637–1071
Cloud base height (m)	849	252	583–1208	804	371	462–1448
Lifting condensation level (m)	629	137	454–812	570	127	405–731
Latent energy flux ($\mathrm{W\,m^{-2}}$)	79.8	56.2	11.4–148.9	70.6	64.2	6.9–135.4

Table 4. Average surface values for low, medium, and high pollution for dry conditions (cases L, M, and H respectively). The numbers in parentheses indicate one standard deviation of the minute-averaged values for which PWV $< 40\,\mathrm{kg\,m^{-2}}$ and CPC $< 1000\,\mathrm{cm^{-3}}$ (low pollution), $1000 <$ CPC $< 1500\,\mathrm{cm^{-3}}$ (medium pollution), or CPC $> 1500\,\mathrm{cm^{-3}}$ (high pollution). Due to the non-normal distributions of many of these parameters, the 10th and 90th percentile ranges are additionally shown (second line). LWP and cloud base height are the averages over cloud events only, as is boundary layer height, to illustrate the position of cloud relative to the boundary layer. Lifting condensation level is calculated from the approximation given in Lawrence (2005). ~~Nighttime~~ Eddy covariance calculations require a 30-minute averaging period; additionally, eddy covariance fluxes were unresolvable during nighttime due to the low wind speeds~~; thus~~. Thus the values of LEF below are for 30-minute-averaged daytime fluxes (6 a.m.–6 p.m. MVT) only. The corresponding 24 h values are 98.5 ± 63.4 (37.4–169.3), 70.4 ± 51.5 (5.2–127.8), and 61.0 ± 42.1 (3.3–113.1) $\mathrm{W\,m^{-2}}$ for cases L, M, and H, respectively.

	Case L low, dry	Case M med, dry	Case H high, dry
Number of cloud events	45	129	89
Cloud LWP ($\mathrm{g\,m^{-2}}$)	97.5 (19.7) 75.0–121.8	145 (22.3) 105.2–163.8	175 (29.2) 109.0–293.6
PWV ($\mathrm{kg\,m^{-2}}$)	29.4 (4.2) 23.5–34.5	31.9 (4.9) 25.4–38.9	31.2 (4.2) 26.0–37.0
CPC ($\mathrm{cm^{-3}}$)	767.7 (118.9) 596–944	1319.9 (136.9) 1138–1487	1673.9 (169.8) 1512–1926
$\mathrm{AOD_{500}}$	0.38 (0.28) 0.14–0.82	0.47 (0.13) 0.26–0.64	0.50 (0.06) 0.45–0.56
Wind speed ($\mathrm{m\,s^{-1}}$)	2.86 (1.20) 1.43–4.56	2.31 (1.31) 0.77–4.25	1.84 (1.01) 0.59–3.17
Surface temperature (°C)	27.97 (0.88) 26.84–29.02	28.64 (0.89) 27.67–30.07	28.80 (1.00) 27.65–30.26
Surface pressure (hPa)	1006.5 (1.3) 1004.9–1008.4	1008.0 (1.8) 1005.4–1010.3	1009.0 (1.7) 1006.8–1011.3
Relative humidity (%)	69.7 (4.2) 63.0–76.7	76.4 (4.2) 70.4–81.2	77.4 (4.6) 71.3–83.5
Specific humidity ($\mathrm{g\,kg^{-1}}$)	16.4 (1.2) 15.1–18.3	18.7 (0.9) 17.6–19.8	19.1 (0.9) 17.9–20.3
Boundary layer height (m)	1270 (173) 1009–1460	912 (161) 667–1054	784 (84) 669–863
Cloud base height (m)	1159 (165) 882–1290	848 (268) 595–1288	820 (203) 590–1077
Lifting condensation level (m)	775 (139) 597–952	608 (110) 481–765	583 (122) 423–746
Latent energy flux ($\mathrm{W\,m^{-2}}$)	113.9 (66.4) 55.7–193.9	74.3 (54.4) 5.5–149.4	64.6 (40.6) 12.7–113.1

Table A1. Trade cumulus cloud properties as measured in previous studies.

Study	cloud base	cloud top	cloud width	cloud lifetime	updraft velocity	LWC
Malkus (1956)[a]	705 m	1.2–1.8 km			3–6 cm s^{-1}	
Malkus (1957)[a]	200–3000 m thick		100–2000 m		0.5–5 m s^{-1}	
Warner (1955)[b]	0.8–1.4 km	2.6–3.3 km	$>$ 600 m	$>$ 30 min		0.4–1.4 g m^{-3}
Simpson and Dennis (1972)[c]	500 m	3 km	500 m	5–10 min	2–3 m s^{-1}	1–3 g m^{-3}
Augstein et al (1974)[d]	600 m	1.3–2 km				
Garstang and Betts (1974)[e]	950 m	2300 m				
MacPherson and Isaac (1977)[f]	1700 m	4400 m	3.2 km			
LaMontagne and Telford (1983)[g]	1700 m	2650 m				
Betts (1997)[h]	950 hPa	800 hPa				
French et al (2000)	$\sim$ 900 m	2–2.9 km	1 km	$\sim$ 30 min	4 m s^{-1} (5–7 max)	0.5–2 g m^{-3}
Rodts et al (2003)	500 m	2500 m	10 m-3 km			

[a] Western Atlantic data, 1946 and 1953.
[b] Measured vertically-resolved LWC within a cloud. Column LWP may be derived through vertical integration, yielding values of 800–1400 g m^{-2}.
[c] Clouds are subadiabatic due to entrainment of outside air.
[d] ATEX (1969) experiment in the equatorial Atlantic.
[e] After Malkus (1956). Clouds are capped by an inversion.
[f] Terrestrial (Canadian) cumulus, including some towering cu. Peak w was seen in the downdrafts rather than updrafts.
[g] Terrestrial (South Dakota) cumulus, Aug 1978. Altitudes are reported as above MSL, which is 1200 m below ground level.
[h] For comparison, the heights in hPa correspond to roughly 500 and 1500 m.

Table A2. Adiabatic estimate of cloud liquid water with several different parameters. ΔT refers to the deviation from the L profile at z_{cb} (green line in Fig. A5). The case name refers to the (Temperature)–(Humidity) conditions imposed. H* represents a cloud base height corresponding to Case H, with the additional condition of cloud top height that of Case L (i.e. thicker clouds).

Case	ΔT	z_{cb}	z_{ct}	LWP	Diff from base case
L-L	+0 °C	800 m	1100 m	178.7 g m^{-2}	0 g m^{-2}
H-L	+2.1 °C	800 m	1100 m	200.3 g m^{-2}	21.6 g m^{-2}
L-H	+0 °C	600 m	900 m	195.2 g m^{-2}	16.5 g m^{-2}
H-H	+1.3 °C	600 m	900 m	209.1 g m^{-2}	30.6 g m^{-2}
L-H*	+0 °C	600 m	1100 m	529.1 g m^{-2}	350.4 g m^{-2}

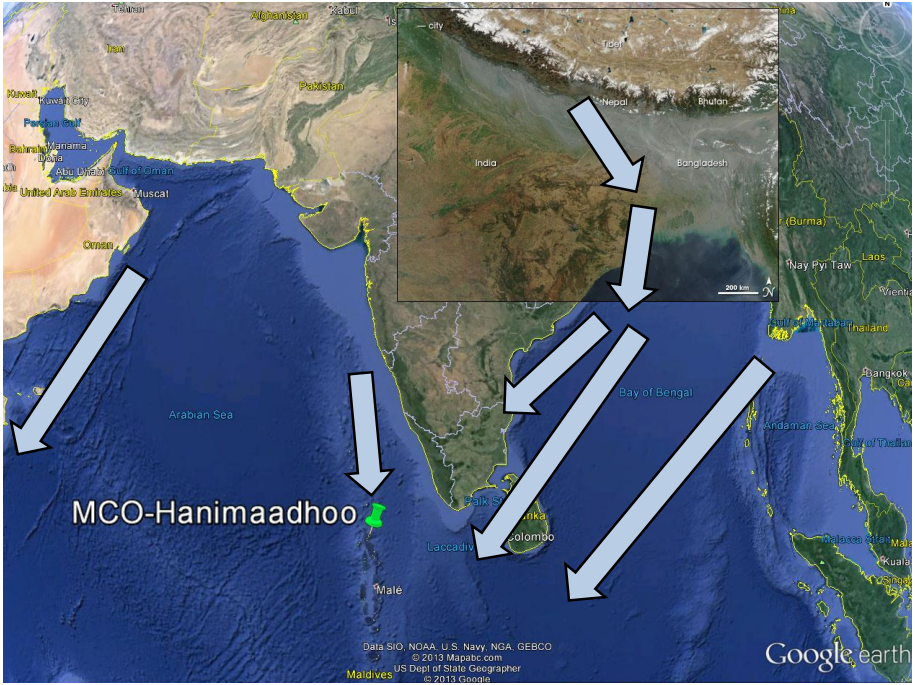

Figure 1. Map of the study location highlighting the Maldives Climate Observatory at Hanimaadhoo (MCOH). The overlay is a NASA MODIS satellite image of the region, showing an aerosol plume coming off the subcontinent. The presence of absorbing aerosols in the plume is evident from its greyish color. Predominant low-level flow during winter months (Lawrence and Lelieveld, 2010) is indicated by the arrows.

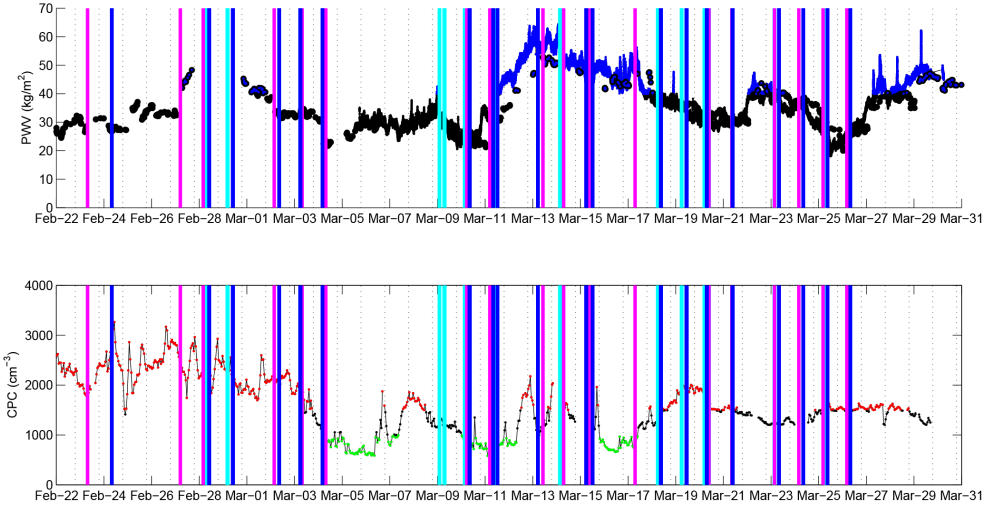

Figure 2. Time series showing the dynamic range of precipitable water vapor (MWR PWV in kg m^{-2}, upper panel) and surface aerosol concentration (CPC number concentration in cm^{-3}, lower panel) observed during CARDEX. The colors correspond to the regimes described in the text: upper panel shows wet (blue) and dry (black) conditions, and lower panel shows low pollution (green) and high pollution (red) conditions. Overlaid vertical lines indicate UAV flight times for the aerosol/radiation (MAC4, magenta), flux (MAC5, blue), and cloud microphysics (MAC6, cyan) planes, showing the wide range of conditions which were sampled.

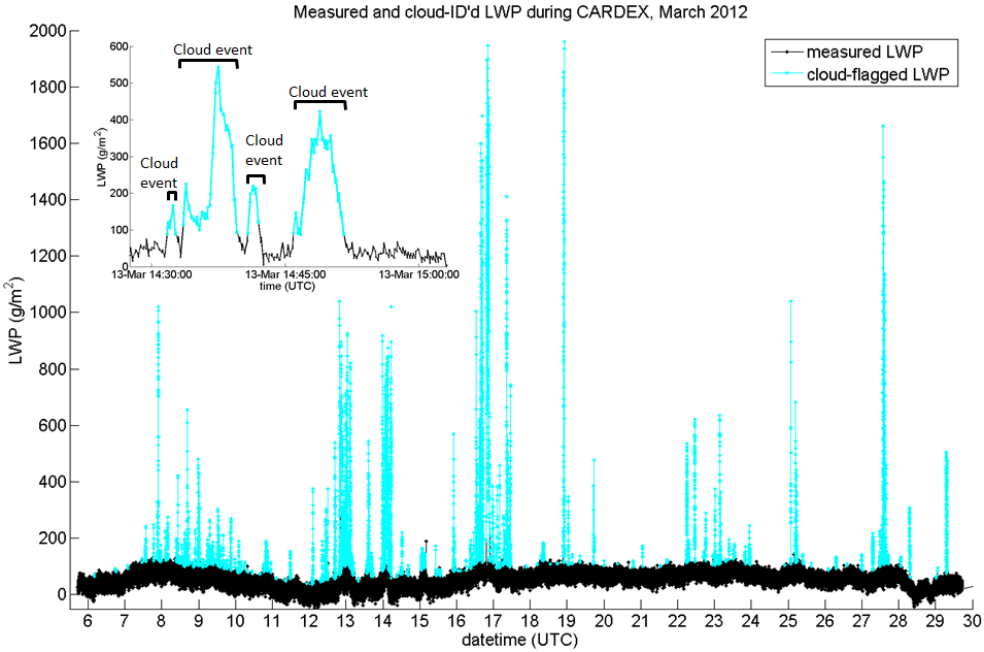

Figure 3. Liquid water path measured by the MWR operated during CARDEX. Cyan points indicate cloud-flagged values, and the inset illustrates an example of cloud "events," as described in Appendix A1.

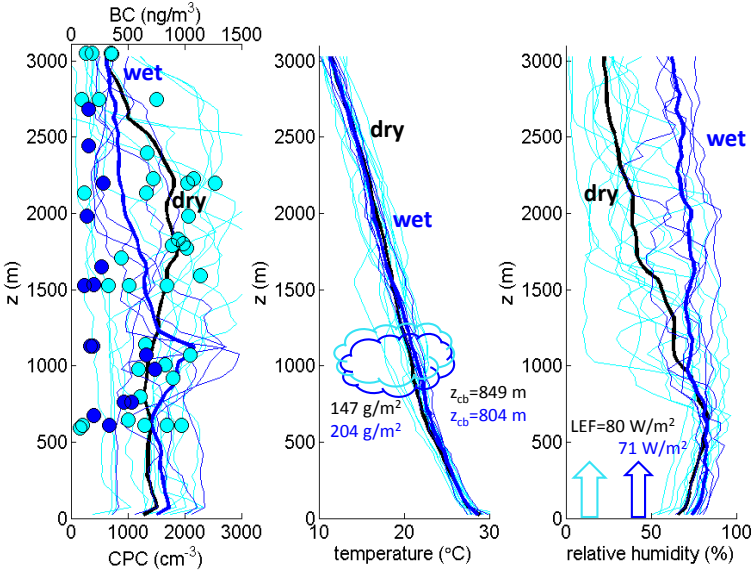

Figure 4. Aerosol, temperature, and relative humidity vertical profiles from the MAC4 aircraft for individual wet (dark blue) and dry (cyan) flights, as indicated by Table 2. The thin lines indicate individual profiles, and the thick lines indicate the ensemble mean. For clarity, the ensemble mean of the dry cases is shown in black. Black carbon retrievals are shown as discrete circles as they required a period of level flight to get an accurate reading. There were 12 dry and 5 wet flights with this aircraft; a description of the flight conditions and times may be found in Table 2. Note that the strong temperature inversion on dry days is most evident in the individual profiles rather than the means, as the latter tends to average out the inversion due to differing boundary layer heights. The average values of liquid water path (LWP), cloud base height (z_{cb}), and latent energy flux (LEF) are measured from the MWR, MPL, and gust probe instrumentation, respectively, at MCOH, and are also shown in Table 3.

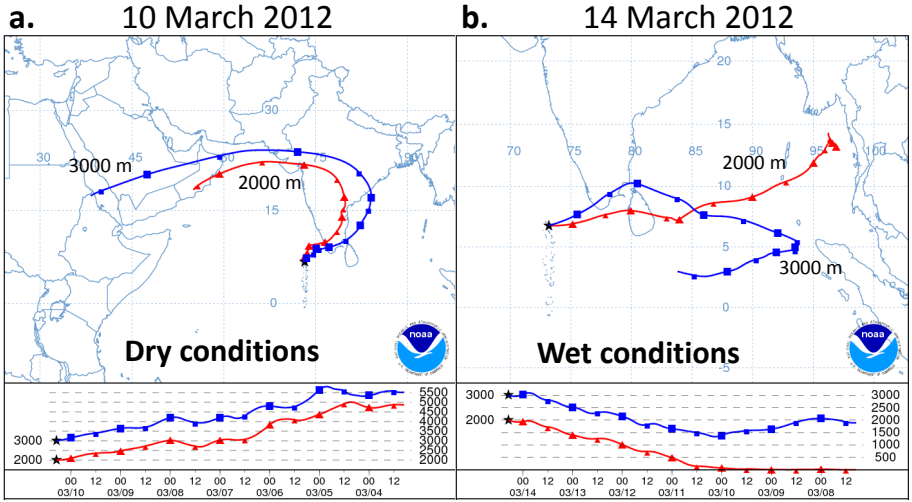

Figure 5. NOAA HYSPLIT 7-day back trajectories arriving at 07:00 Z (12:00 MVT) for **(a)** 10 March 2012, a typical "dry" day, and **(b)** 14 March 2012, a typical "wet" day. Visualization from the HYSPLIT-WEB tool (http://ready.arl.noaa.gov/HYSPLIT.php).

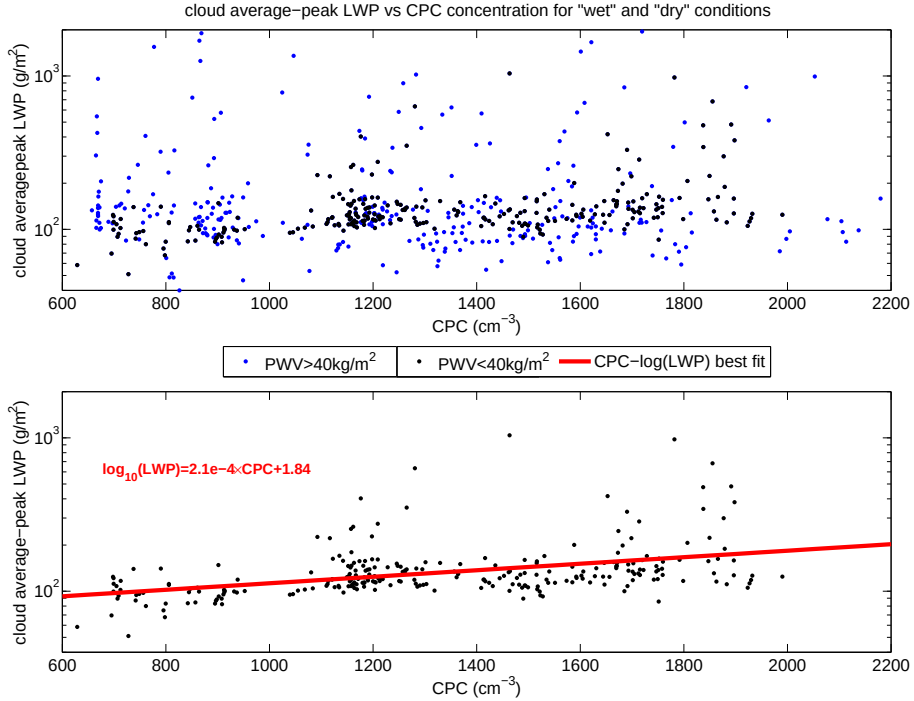

Figure 6. Cloud average-peak liquid water path vs. aerosol concentration, for all clouds (top; wet in blue, dry in black) and just dry condition clouds (bottom). Note the logarithmic scaling on the y axis. The red line indicates the linear best fit between CPC aerosol number concentration and log(LWP).

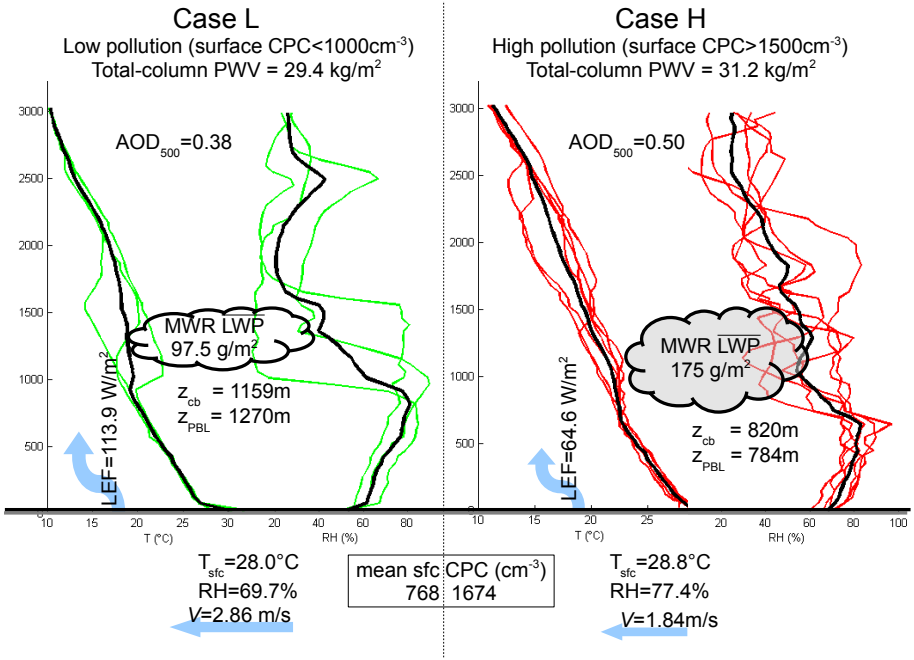

Figure 7. Characteristics of Case L vs. Case H conditions. By definition Case H has higher surface aerosol concentration; as expected, this is also true for AERONET-measured column AOD. Case H also sees higher humidity, lower surface vapor fluxes, and lower wind speed and, as shown by Fig. 6, has greater average cloud LWP. The lidar retrievals of cloud base and boundary layer height and the calculated LCL height are systematically lower for more polluted conditions.

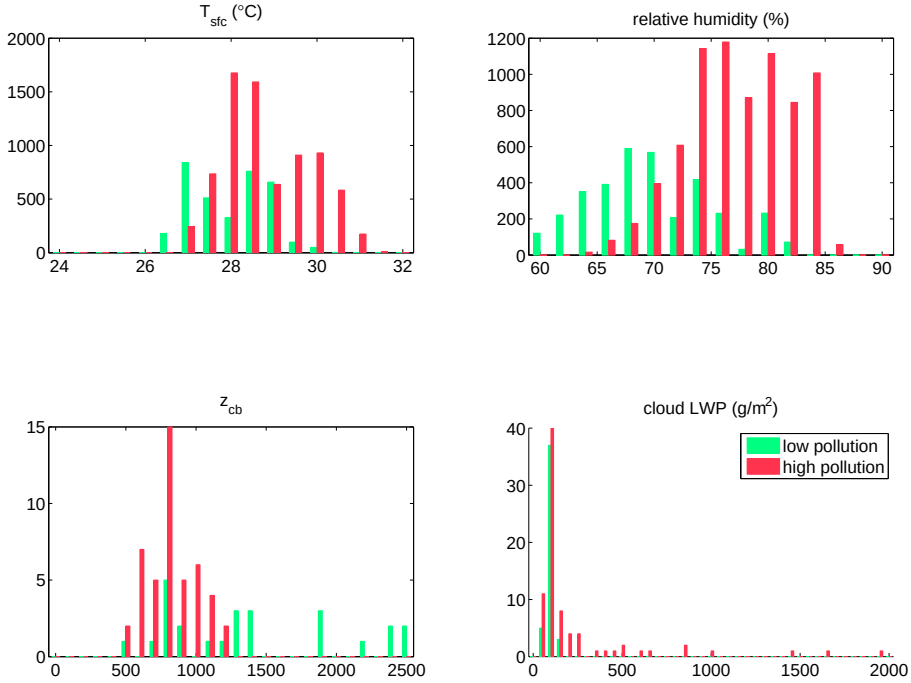

Figure 8. Frequency distributions of surface air temperature and relative humidity (minute data from MCOH), cloud base height (cloud-averaged data from MPL), and cloud liquid water path (cloud-averaged data from MWR) for low vs. high pollution cases.

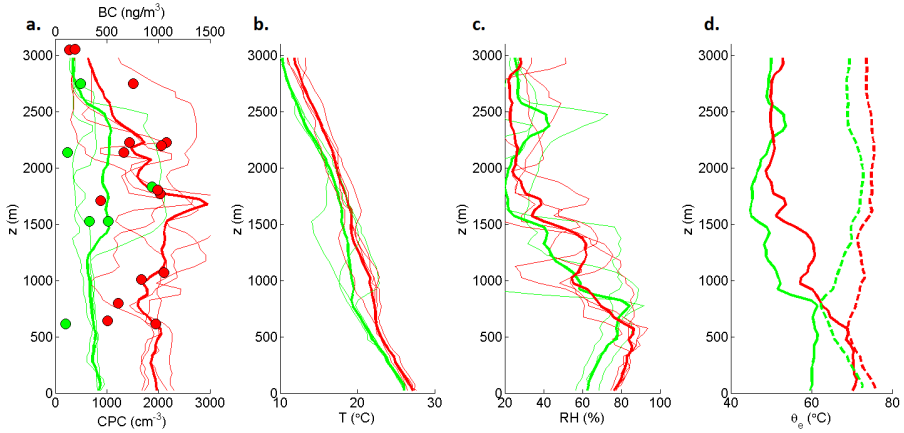

Figure 9. Profiles of **a.** aerosol~~(left)~~, **b.** temperature~~(center)~~, ~~and~~ **c.** relative humidity~~(right)~~, and **d.** equivalent potential temperature θ_e from MAC4 for low (Case L; green) and high (Case H; red) pollution cases. Thin lines indicate the individual flights, and the thick line shows the mean of each case. The saturation equivalent potential temperature θ_e^* is shown as dashed lines in **d**. There were 3 and 5 flights with this aircraft sampling low- and high-pollution dry conditions, respectively. In the left panel, CPC (cm^{-3}) is indicated by lines while BC retrievals ($ng\,m^{-3}$), which required a period of level flight to obtain an accurate measurement, are indicated by colored circles. Case H has significantly higher aerosol concentration at all altitudes, although this does not universally show an elevated aerosol plume. This case is coincident with warmer atmospheric temperatures and higher humidity at all altitudes. ~~The difference between H and L means is shown in Fig. A10.~~Note that due to missing pressure data in two of the MAC4 flights, this calculated variable was determined using two less flights compared with **a-c**.

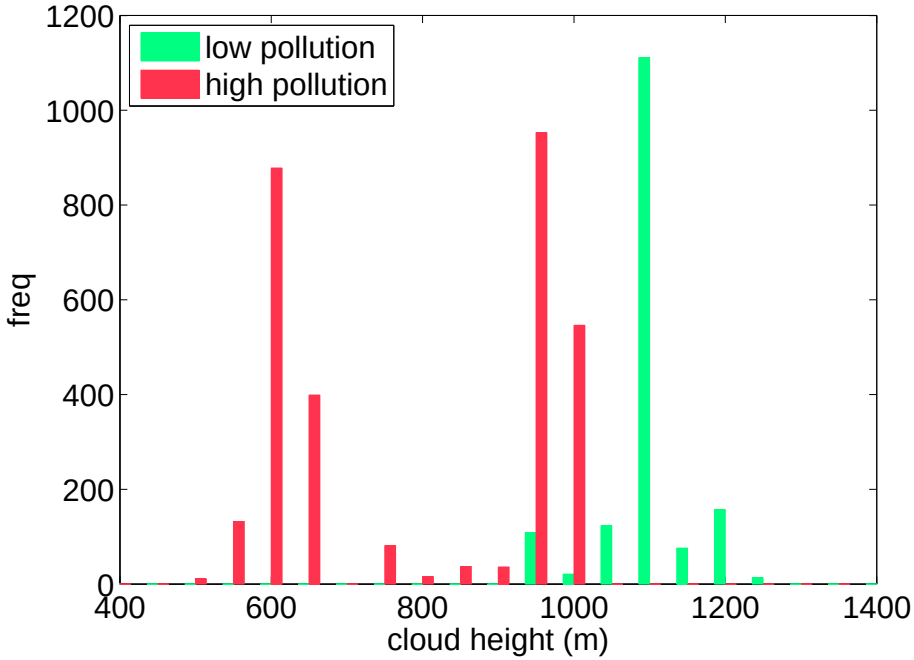

Figure 10. Altitude of cloud retrievals by MAC6 under low (green) and high (red) pollution cases, for 5 high-pollution and 2 low-pollution flights. Note that this figure shows the height at which the aircraft penetrated the clouds rather than cloud base or top height; however, the observations are consistent with overall lower cloud heights under polluted conditions.

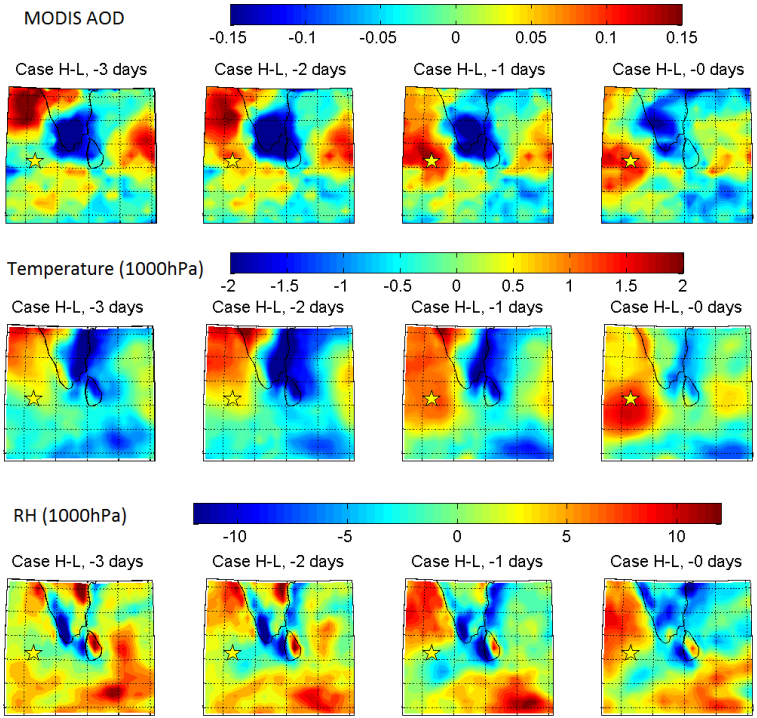

Figure 11. The difference in high minus low pollution conditions for MODIS AOD (top row) and ECMWF temperature (middle row) and relative humidity (bottom row) at 1000 hPa (approximately 75 m) for "dry" days as identified in Table 1. The 1-day lag between maximum AOD and temperature, and maximum relative humidity is evident in the day-to-day progression. Average Case L and Case H conditions overlaid with wind fields are shown in Figs. A6–A8.

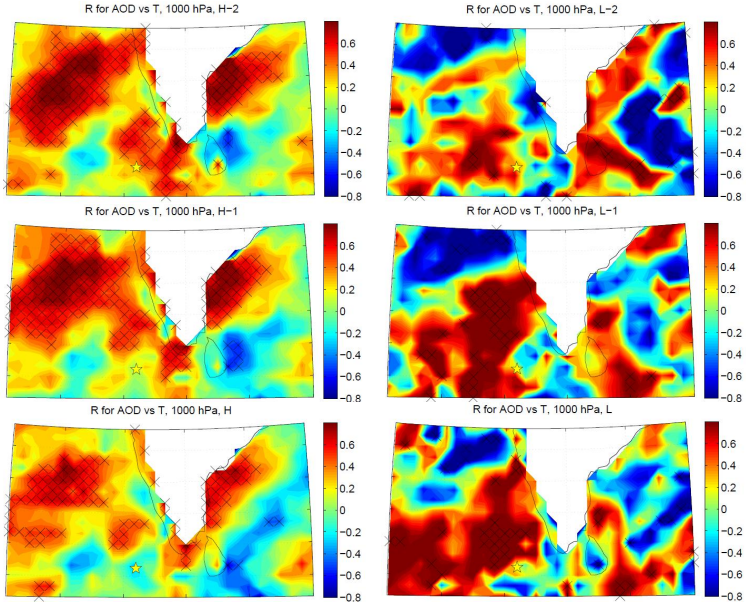

Figure 12. Correlation between AOD and 1000 hPa temperature for days leading up to high- (left) or low-pollution (right) events. The bottom row indicates the average of the days classified as a particular pollution event, while the middle and upper rows indicate the averages of one and two days prior, respectively. Hatching indicates a statistical significance at the 95 % level.

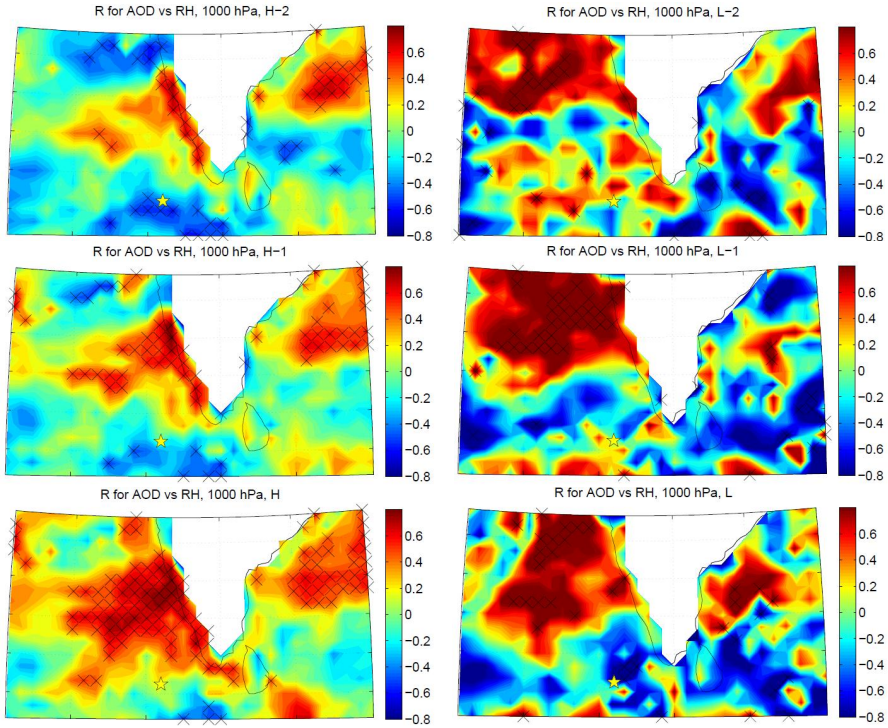

Figure 13. Correlation between MODIS AOD and ECMWF 1000 hPa relative humidity for days leading up to high- (left) or low-pollution (right) events. The bottom row indicates the average of the days classified as a particular pollution event, while the middle and upper rows indicate one and two days prior, respectively. Hatching indicates a statistical significance at the 95 % level.

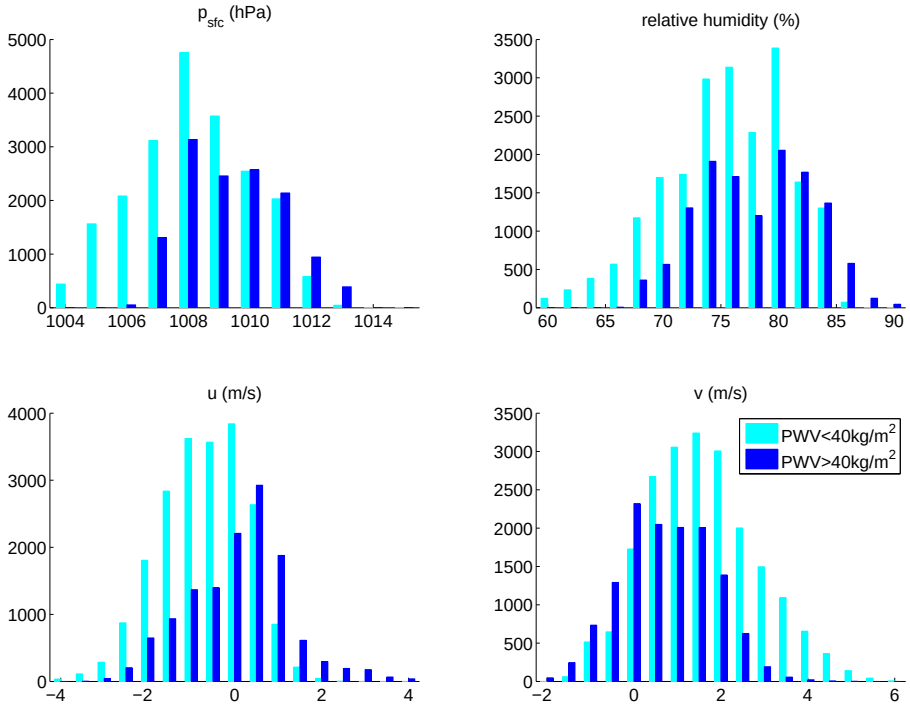

Figure A1. Distributions of MCOH variables on minute-resolution for low (PWV $< 40\,\mathrm{kg\,m^{-2}}$, cyan) and high (PWV $> 40\,\mathrm{kg\,m^{-2}}$, blue) water vapor conditions. Dry cases on average correspond to a lower surface pressure, lower surface humidity, and faster surface wind speed in both north/south (northerly) and east/west (westerly) directions.

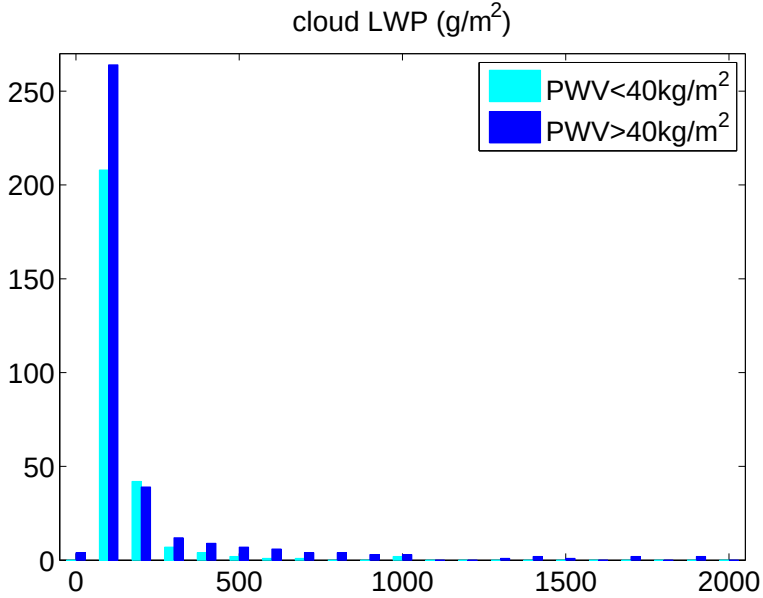

Figure A2. Frequency distribution of cloud LWP for wet (dark blue) and dry (cyan) cases. The clouds under the wet case exhibit more variability in water content than do clouds observed under dry conditions (Table 3), possibly due to a lack of a well-defined boundary layer topped by a temperature inversion, which would act to limit cloud vertical development as in the “dry” cases.

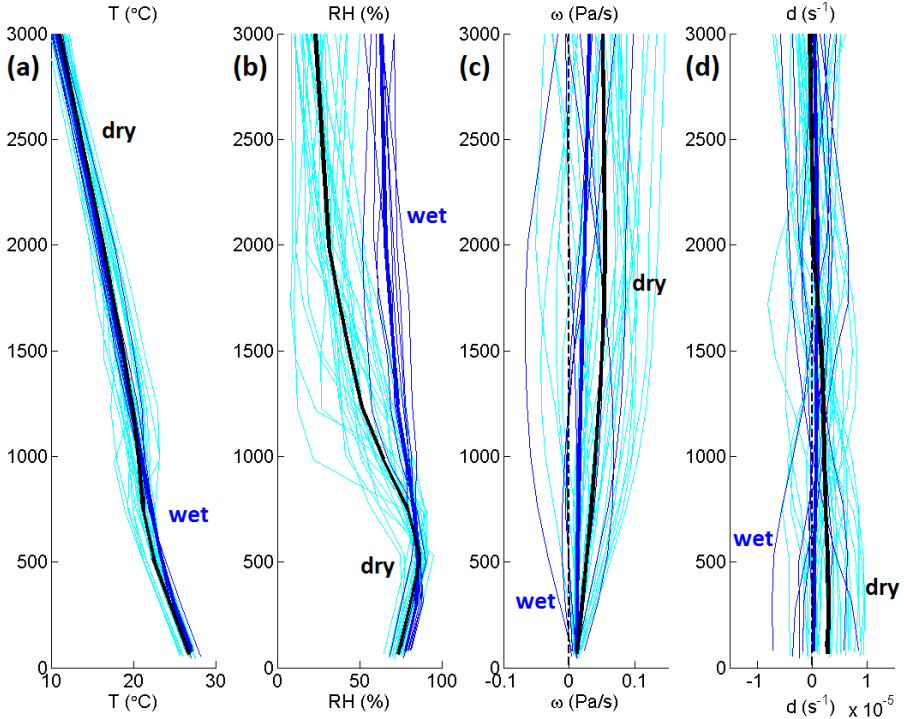

Figure A3. ECMWF temperature, relative humidity, pressure vertical velocity, and divergence over MCOH for wet (thin blue, mean in thick blue) vs. dry (thin cyan, mean in thick black) days during CARDEX. (**a** and **b**) exhibit good agreement with the observed vertical profiles measured by the aircraft: as in the flight data, the dry days exhibit a stronger temperature inversion and subsequent drop in humidity, whereas wet cases have consistently higher humidity above the 1000–1500 m inversion. Also consistent with the back trajectory analysis, there is stronger **(c)** subsidence and corresponding **(d)** divergence for the dry cases.

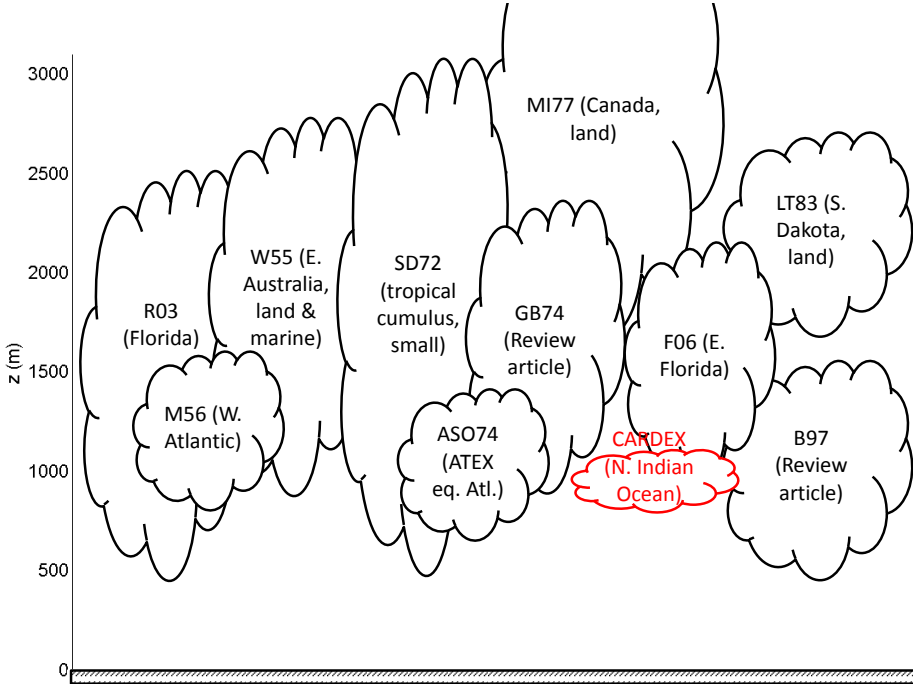

Figure A4. Previous descriptions of small cumulus according to the literature. Note that some clouds, especially those measured over land, are physically larger than the clouds observed in the Indian Ocean during CARDEX. References are those in Table A1.

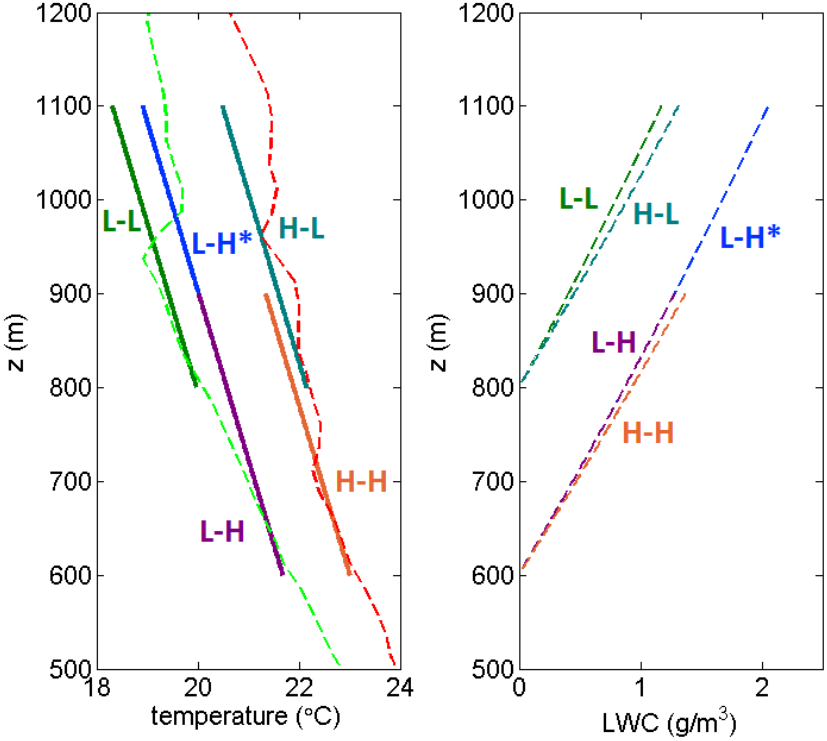

Figure A5. Adiabatic temperature profiles (left) and CLWC profiles (right) for the cases described in the text. Numerical values are given in Table A2.

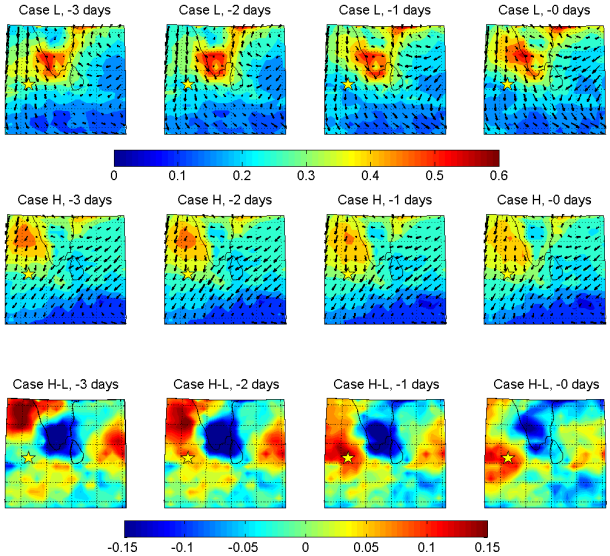

Figure A6. Average daily MODIS AOD for (top row) Case L, (middle row) Case H, and (bottom row) the difference between the two. Note that this includes all Case L and Case H days as identified in Table 1, rather than solely the ones on which a UAV was flown. The color scale shown is the same for both Case L and Case H, and the location of MCOH is indicated by the yellow star. From left to right, the columns are 0, 1, 2, or 3 days prior to a given classification. Note that while Case H corresponds to higher AOD over MCOH, Case L sees higher AOD over the Indian subcontinent. In Case H, the air mass of high aerosol concentration is seen to move south-southeastward to arrive over MCOH. This corresponds to the HYSPLIT and ECMWF low-level trajectories, indicating that upper-level pollution transport is not dominant in these cases. The arrows overlaid on the top two rows indicate the ECMWF average wind fields at 1000 hPa, showing similar north-northwesterly flow approaching MCOH in both cases. With increasing altitude, the wind can be seen to change to a northeasterly direction around the 850 hPa level, although this change occurs lower in altitude for Case H ($\sim$ 900 vs. $\sim$ 800 hPa).

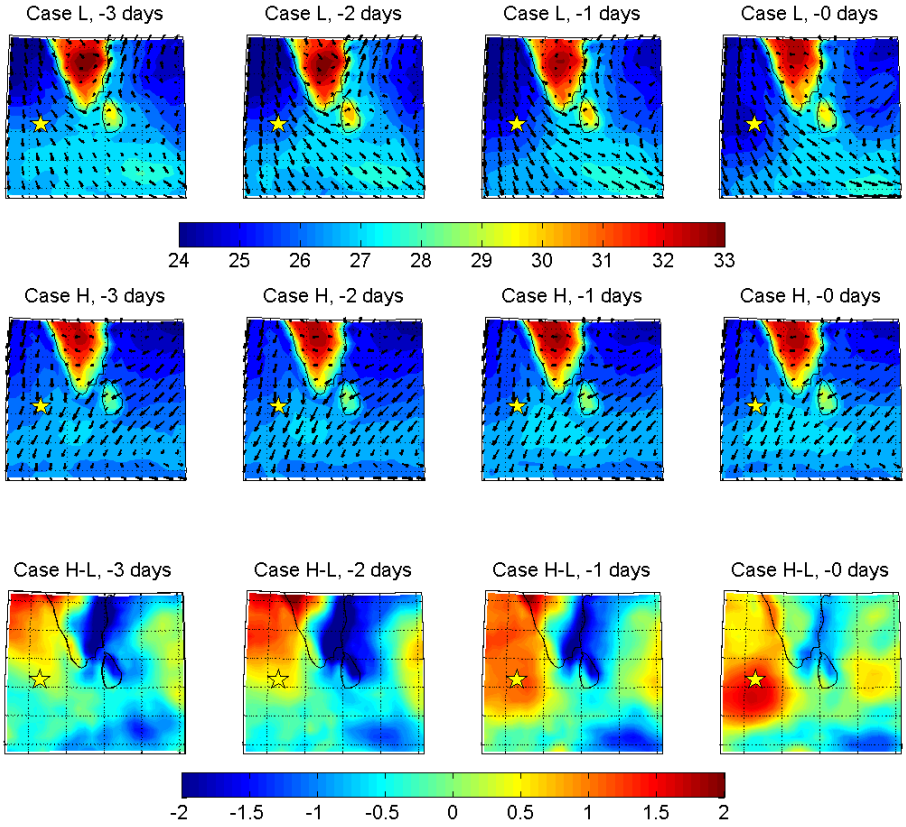

Figure A7. As in Fig. A6, but showing ECMWF 1000 hPa temperature (°C) for Case L, Case H, and the difference (H-L) for 3, 2, 1, and 0 days prior, overlaid with average winds.

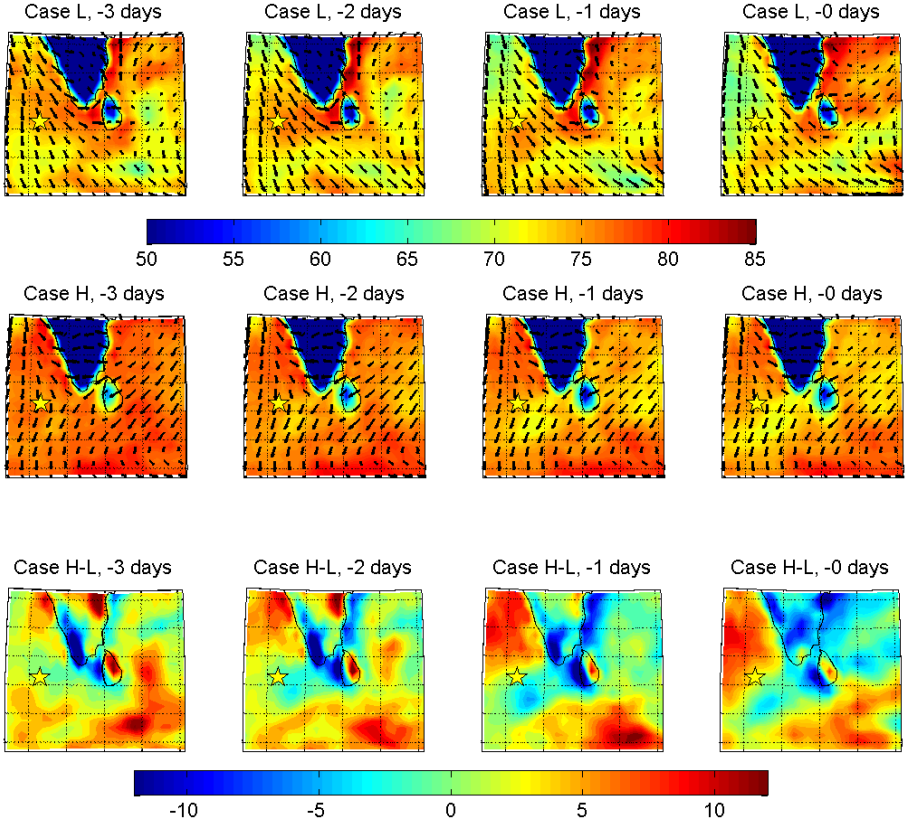

Figure A8. As in Figs. A6 and A7, but showing ECMWF 1000 hPa relative humidity (%) for Case L, Case H, and the difference (H-L) for 3, 2, 1, and 0 days prior, overlaid with average winds.

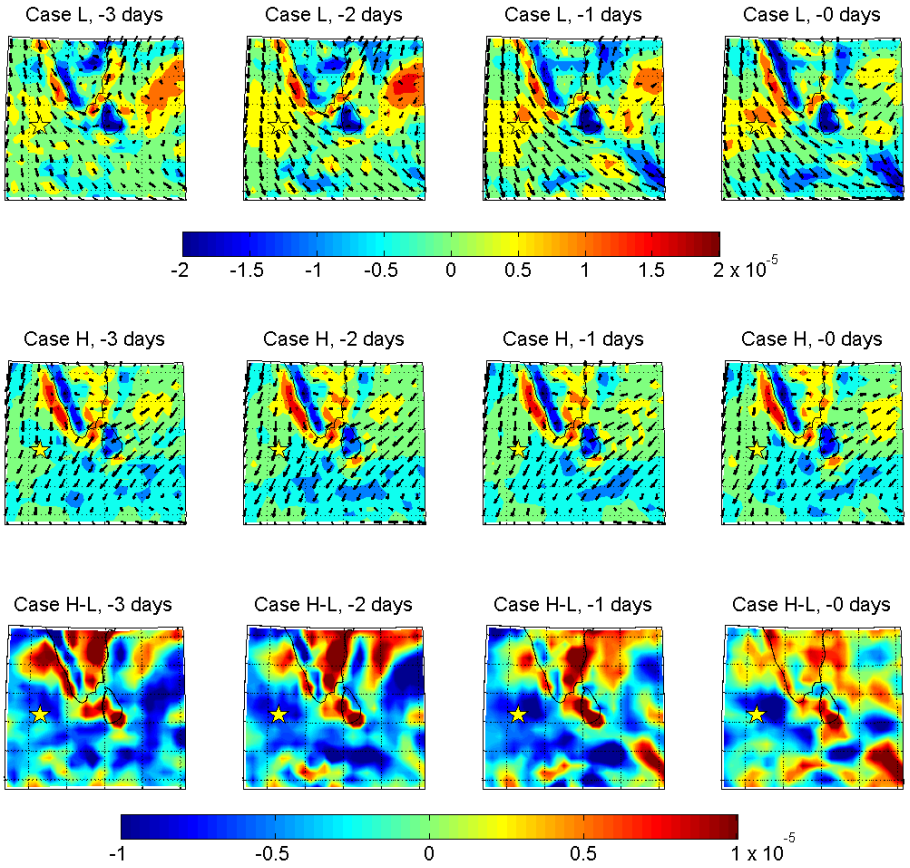

Figure A9. As in Figs. A6 through A8, showing ECMWF 1000 hPa divergence (s^{-1}) for Case L, Case H, and the difference (H-L) for 3, 2, 1, and 0 days prior, overlaid with average winds.

DELETED FIGURES

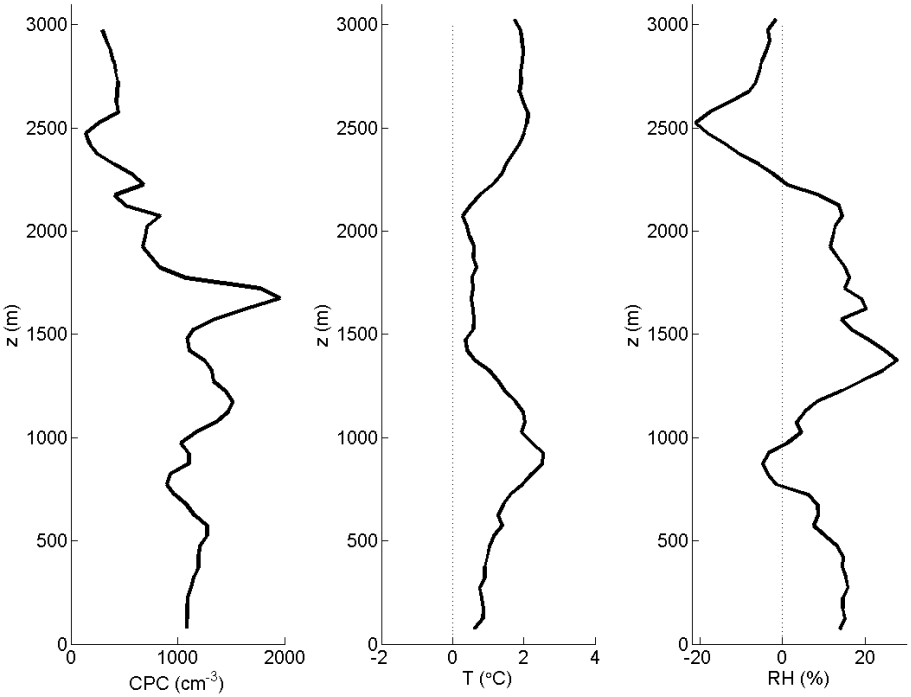

Figure A10. ~~As in Fig. 9, here illustrating the H-L differences in measured MAC4 profiles of CPC, temperature, and relative humidity.~~

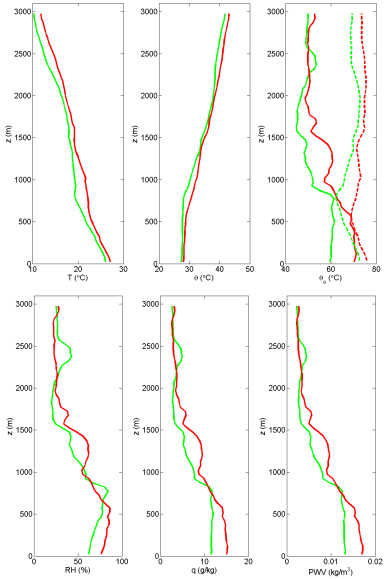

Figure A11. MAC4 vertical profiles for low (green) and high (red) pollution cases. The saturation equivalent potential temperature θ_e^*, is shown as dashed lines in the top right panel. Note that due to missing pressure data in two of the MAC4 flights, the calculated variables are determined using two less flights compared with Figs. 9 to 7. For consistency, these T and RH plots use the same data as in the calculated panels, and while the mean profiles are quantitatively slightly different, the high/low difference is essentially unchanged. Also of note is that the relative humidity increase with altitude between the surface and the top of the boundary layer appears to be primarily due to the change in temperature, as q remains fairly constant within this range. This is a product of the more strongly-defined boundary layer top with a sharp drop in RH for Case L. Whereas the RH of Case H decreases more slowly even for individual flights, the Case L average is higher than H just at the height of the Case L boundary layer top. This is less pronounced in q or PWV due to the coincident temperature inversion.